International Ocean Discovery Program Expedition 366 Preliminary Report

Mariana Convergent Margin and South Chamorro Seamount

8 December 2016 to 7 February 2017

Patricia Fryer, Geoffrey Wheat, Trevor Williams, and the Expedition 366 Scientists

IODP
INTERNATIONAL OCEAN DISCOVERY PROGRAM

Publisher's notes

Core samples and the wider set of data from the science program covered in this report are under moratorium and accessible only to Science Party members until 7 February 2018.

This publication was prepared by the *JOIDES Resolution* Science Operator (JRSO) at Texas A&M University (TAMU) as an account of work performed under the International Ocean Discovery Program (IODP). Funding for IODP is provided by the following international partners:

National Science Foundation (NSF), United States
Ministry of Education, Culture, Sports, Science and Technology (MEXT), Japan
European Consortium for Ocean Research Drilling (ECORD)
Ministry of Science and Technology (MOST), People's Republic of China
Korea Institute of Geoscience and Mineral Resources (KIGAM)
Australia-New Zealand IODP Consortium (ANZIC)
Ministry of Earth Sciences (MoES), India
Coordination for Improvement of Higher Education Personnel (CAPES), Brazil

Portions of this work may have been published in whole or in part in other IODP documents or publications.

Disclaimer

Copyright

Citation

Fryer, P., Wheat, G., Williams, T., and the Expedition 366 Scientists, 2017. *Expedition 366 Preliminary Report: Mariana Convergent Margin and South Chamorro Seamount*. International Ocean Discovery Program. https://doi.org/10.14379/iodp.pr.366.2017

ISSN
World Wide Web: 2372-9562

Expedition 366 participants

Expedition 366 scientists

Patricia B. Fryer
Co-Chief Scientist
Hawaii Institute of Geophysics and Planetology/SOEST
University of Hawaii at Manoa
USA
pfryer@soest.hawaii.edu

C. Geoffrey Wheat
Co-Chief Scientist
College of Fisheries and Ocean Sciences
University of Alaska Fairbanks
USA
wheat@mbari.org

Trevor Williams
Expedition Project Manager/Staff Scientist
International Ocean Discovery Program
Texas A&M University
USA
williams@iodp.tamu.edu

Elmar J. Albers
Core Description
Department of Geosciences
University of Bremen
Germany
e.albers@uni-bremen.de

Barbara Bekins
Petrophysics Specialist/ Downhole Tools Specialist
Water Resources
United States Geological Survey
USA
babekins@usgs.gov

Vitor Magalhaes
Physical Properties Specialist
Marine Geology and Georesources
Instituto Português do Mar e da Atmosfera
Portugal
vitor.magalhaes@ipma.pt

Baptiste P.R. Debret
Core Description
Department of Earth Sciences
University of Cambridge
United Kingdom
ba.debret@gmail.com

Jianghong Deng
Core Description
School of Earth and Space Sciences
University of Science and Technology of China
China
jhdeng0507@163.com

Yanhui Dong
Core Description
Key Laboratory of Submarine Geoscience
Second Institute of Oceanography, State Oceanic Administration
China
luster15991@163.com

Philip Eickenbusch
Microbiologist
Department of Environmental Systems Science
ETH Zurich
Switzerland
philip.eickenbusch@usys.ethz.ch

Emanuelle A. Frery
Core Description
Commonwealth Scientific and Industrial Research Organisation
Australia
emanuelle.frery@csiro.au

Yuji Ichiyama
Core Description
Department of Earth Sciences
Chiba University
Japan
ichiyamay@earth.s.chiba-u.ac.jp

Kevin Johnson
Core Description
Department of Geology and Geophysics
University of Hawaii at Mānoa
USA
kjohnso2@hawaii.edu

Raymond M. Johnston
Core Description
School of Geosciences
University of South Florida, Tampa
USA
raymj@tampabay.rr.com

Richard T. Kevorkian
Microbiologist
Department of Microbiology
University of Tennessee
USA
rtkevork@gmail.com

Walter Kurz
Igneous Petrologist/Metamorphic Petrologist
Institute of Earth Sciences
University of Graz
Austria
walter.kurz@uni-graz.at

Simone S. Mantovanelli
Paleomagnetist
Oceanographic Institute of São Paulo University
Brazil
sonvesso@gmail.com

Walter Menapace
Petrophysics Specialist
Marine Engineering Geology/Marine Geotechnics
University of Bremen
Germany
wmenapace@marum.de

Catriona D. Menzies
Inorganic Geochemist
Ocean and Earth Science
National Oceanography Centre
University of Southampton
United Kingdom
c.menzies@soton.ac.uk

Katsuyoshi Michibayashi
Core Description
Institute of Geosciences
Shizuoka University
Japan
michibayashi@shizuoka.ac.jp

Craig L. Moyer
Microbiologist
Biology Department
Western Washington University
USA
cmoyer@hydro.biol.wwu.edu

Kelli K. Mullane
Microbiologist
Scripps Institution of Oceanography
University of California, San Diego
USA
kmullane@ucsd.edu

Jung-Woo Park
Core Description
School of Earth and Environmental Sciences
Seoul National University
Republic of Korea
jung-woo.park@snu.ac.kr

Roy E. Price
Inorganic Geochemist
School of Marine and Atmospheric Sciences
State University of New York, Stony Brook
USA
roy.price@stonybrook.edu

Jeffrey G. Ryan
Inorganic Geochemist
School of Geosciences
University of South Florida, Tampa
USA
ryan@mail.usf.edu

John W. Shervais
Igneous Petrologist
Department of Geology
Utah State University
USA
john.shervais@usu.edu

Olivier J. Sissmann
Organic Geochemist
IFP Energies Nouvelles
France
olivier.sissmann@ifpen.fr

Shino Suzuki
Microbiologist
Japan Agency for Marine-Earth Science and Technology
Japan
sisuzuki@jamstec.go.jp

Ken Takai
Microbiologist
Subground Animalcule Retrieval Project
Japan Agency for Marine-Earth Science and Technology
Japan
kent@jamstec.go.jp

Bastien Walter
Petrophysics Specialist
Ecole Nationale Superieure de Geologie
Universite de Lorraine
France
bastien.walter@univ-lorraine.fr

Rui Zhang
Microbiologist
State Key Laboratory of Marine Environmental Sciences
Xiamen University
China
ruizhang@xmu.edu.cn

Education/Outreach Officers

Martin Böttcher
Rabanus-Maurus-Schule
Fulda
Germany
mboceanethics@gmail.com

Kristen Weiss
Center for Ocean Solutions
Stanford University
USA
kristencheriweiss@gmail.com

Siem offshore AS officials

Steve Bradley
Master of the Drilling Vessel

Wayne Malone
Offshore Installation Manager

JRSO shipboard personnel and technical representatives

Timothy Blaisdell
Applications Developer

Lisa Brandt
Chemistry Laboratory

Lisa Crowder
Assistant Laboratory Officer

Aaron de Loach
Core Laboratory

Keith Dupuis
Underway Geophysics Laboratory

Timothy Fulton
Imaging Specialist

Clayton Furman
Schlumberger Logging Engineer

Randy Gjesvold
Marine Instrumentation Specialist

Sandra Herrmann
Assistant Laboratory Officer

Michael Hodge
Marine Computer Specialist

Jon Howell
Applications Developer

Minh Nhut Huynh
Marine Computer Specialist

Rhonda Kappler
Publications Specialist

Nicolette Lawler
X-Ray Laboratory

Brittany Martinez
Curatorial Specialist

Aaron Mechler
Chemistry Laboratory

Mike Meiring
Electronics Specialist

William Mills
Laboratory Officer

Beth Novak
Paleomagnetism Laboratory

Bill Rhinehart
Drilling Engineer

Patrick Riley
Core Laboratory (temporary)

Michael Storms
Operations Superintendent

Johanna Suhonen
Thin Section Laboratory (temporary)

Garrick Van Rensburg
Marine Instrumentation Specialist

Abstract

Geologic processes at convergent plate margins control geochemical cycling, seismicity, and deep biosphere activity in subduction zones and suprasubduction zone lithosphere. International Ocean Discovery Program (IODP) Expedition 366 was designed to address the nature of these processes in the shallow to intermediate depth of the Mariana subduction channel. Although no technology is available to permit direct sampling of the subduction channel of an intraoceanic convergent margin at depths up to 18 km, the Mariana forearc region (between the trench and the active volcanic arc) provides a means to access this zone.

Active conduits, resulting from fractures in the forearc, are prompted by along- and across-strike extension that allows slab-derived fluids and materials to ascend to the seafloor along associated faults, resulting in the formation of serpentinite mud volcanoes. Serpentinite mud volcanoes of the Mariana forearc are the largest mud volcanoes on Earth. Their positions adjacent to or atop fault scarps on the forearc are likely related to the regional extension and vertical tectonic deformation in the forearc. Serpentinite mudflows at these volcanoes include serpentinized forearc mantle clasts, crustal and subducted Pacific plate materials, a matrix of serpentinite muds, and deep-sourced formation fluid. Mud volcanism on the Mariana forearc occurs within 100 km of the trench, representing a range of depths and temperatures to the downgoing plate and the subduction channel. These processes have likely been active for tens of millions of years at this site and for billions of years on Earth.

At least 10 active serpentinite mud volcanoes have been located in the Mariana forearc. Two of these mud volcanoes are Conical and South Chamorro Seamounts, which are the furthest from the Mariana Trench at 86 and 78 km, respectively. Both seamounts were cored during Ocean Drilling Program (ODP) Legs 125 and 195, respectively. Data from these two seamounts represent deeper, warmer examples of the continuum of slab-derived materials as the Pacific plate subducts, providing a snapshot of how slab subduction affects fluid release, the composition of ascending fluids, mantle hydration, and the metamorphic paragenesis of subducted oceanic lithosphere. Data from the study of these two mud volcanoes constrain the pressure, temperature, and composition of fluids and materials within the subduction channel at depths of about 18 to 19 km. Understanding such processes is necessary for elucidating factors that control seismicity in convergent margins, tectonic and magma genesis processes in the forearc and volcanic arc, fluid and material fluxes, and the nature and variability of environmental conditions that impact subseafloor microbial communities.

Expedition 366 centered on data collection from cores recovered from three serpentinite mud volcanoes that define a continuum of subduction-channel processes defined by the two previously cored serpentinite mud volcanoes and the trench. Three serpentinite mud volcanoes (Yinazao, Fantangisña, and Asùt Tesoro) were chosen at distances 55 to 72 km from the Mariana Trench. Cores were recovered from active sites of eruption on their summit regions and on the flanks where ancient flows are overlain by more recent ones. Recovered materials show the effects of dynamic processes that are active at these sites, bringing a range of materials to the seafloor, including materials from the lithosphere of the Pacific plate and from subducted seamounts (including corals). Most of the recovered material consists of serpentinite mud containing lithic clasts, which are derived from the underlying forearc crust and mantle and the subducting Pacific plate. Cores from each of the three seamounts drilled during Expedition 366, as well as those from Legs 125 and 195, include material from the underlying Pacific plate. A thin cover of pelagic sediment was recovered at many Expedition 366 sites, and at Site U1498 we cored through serpentinite flows to the underlying pelagic sediment and volcanic ash deposits. Recovered serpentinites are largely uniform in major element composition, with serpentinized ultramafic rocks and serpentinite muds spanning a limited range in SiO_2, MgO, and Fe_2O_3 compositions. However, variation in trace element composition reflects pore fluid composition, which differs as a function of the temperature and pressure of the underlying subduction channel. Dissolved gases H_2, CH_4, and C_2H_6 are highest at the site furthest from the trench, which also has the most active fluid discharge of the Expedition 366 serpentinite mud volcanoes. These dissolved gases and their active discharge from depth likely support active microbial communities, which were the focus of in-depth subsampling and preservation for shore-based analytical and culturing procedures. The effects of fluid discharge were also registered in the porosity and GRA density data indicated by higher than expected values at some of the summit sites. These higher values are consistent with overpressured fluids that minimize compaction of serpentinite mud deposits. In contrast, flank sites have significantly greater decreases in porosity with depth, suggesting that processes in addition to compaction are required to achieve the observed data. Thermal measurements reveal higher heat flow values on the flanks (~31 mW/m^2) than on the summits (~17 mW/m^2) of the seamounts. The new 2G Enterprises superconducting rock magnetometer (liquid helium free) revealed relatively high values of both magnetization and bulk magnetic susceptibility of discrete samples related to ultramafic rocks, particularly in dunite. Magnetite, a product of serpentinization, and authigenic carbonates were observed in the mudflow matrix materials.

In addition to coring operations, Expedition 366 focused on the deployment and remediation of borehole casings for future observatories and set the framework for in situ experimentation. Borehole work commenced at South Chamorro Seamount, where the original-style CORK was partially removed. Work then continued at each of the three summit sites following coring operations. Cased boreholes with at least three joints of screened casing were deployed, and a plug of cement was placed at the bottom of each hole. Water samples were collected from two of the three boreholes, revealing significant inputs of formation fluids. This suggests that each of the boreholes tapped a hydrologic zone, making these boreholes suitable for experimentation with the future deployment of a CORK-lite.

An active education and outreach program connected with many classrooms on shore and with the general public through social media.

Background

Geologic processes at convergent plate margins affect geochemical cycling and fluxes, seismicity and natural hazards, crustal and mantle evolution and mixing, and biosphere activity and population dynamics in subduction zones. To constrain these processes, one needs to quantify the inputs and outputs. Quantifying inputs into a convergent plate margin is accomplished by sampling the downgoing plate prior to subduction, providing a geochemical, physical, and mechanical reference. The study of the output in terms of magma and volatiles in volcanic arcs and in backarc basin settings constrains processes that occur deep within the subduction zone,

but such studies of subduction systems are incomplete, lacking an understanding of processes that occur between the time the subducting plate enters the trench and the time it reaches the zone of magma genesis beneath the arc. The Mariana convergent system provides a window into this zone.

The Mariana convergent system is a nonaccretionary-type convergent plate margin (Uyeda and Kanamori, 1979). Here, fluids and materials rise from the subducted Pacific plate within long-lived permeable pathways through the overlying Philippine plate. Such pathways are maintained with across- and along-strike extension (Fryer and Salisbury, 2006). Vertical tectonic deformation is another potential process that shapes fault patterns in the forearc. Vertical deformation occurs when Cretaceous Pacific plate guyots are subducted. In contrast, the zone between the trench and the region of arc magmagenesis is not accessible in accretionary forearcs. Here, deep-sourced fluids ascend through imbricate fault systems and splays in an accretionary prism. Transit of deep-sourced fluids through the prism result in a reaction with a compositionally heterogeneous package of accreted sediments, obfuscating the composition of the deep-sourced fluid. Thus, the Mariana forearc region is unique in the world today, in that it provides direct access to deep-sourced fluids and material from the subduction channel and supra-subduction zone via active serpentinite mud volcanism. Furthermore, ascending deep-sourced fluids, with elevated pH, methane, and hydrogen concentrations relative to seawater, support subsurface microbial communities. Such fluids vent at summit seeps, sometimes supporting megafaunal communities (Fryer, 2011; Ohara et al., 2010).

Therefore, to study processes in the Mariana forearc we chose four active serpentinite mud volcanoes (Yinazao, Fantangisña, Asùt Tesoro, and South Chamorro) for investigation during Expedition 366 (Figure **F1**; Table **T1**). Operations included coring at summit and flank sites on Yinazao, Fantangisña, and Asùt Tesoro Seamounts, deploying a screened casing for future borehole experiments on the summits of each, and revitalizing the borehole observatory (CORK) at South Chamorro Seamount (Ocean Drilling Program [ODP] Site 1200).

Yinazao Seamount (informally called Blue Moon Seamount) lies on the eastern edge of a forearc graben about 55 km from the Mariana Trench axis (Figure **F1**; Table **T1**). Of the three mud volcanoes cored during the expedition, Yinazao Seamount is the closest to the trench, and the subducting slab lies approximately 13 km below its summit (Oakley et al., 2007, 2008). Like the many other serpentinite mud volcanoes that populate the southern half of the Mariana forearc, Yinazao Seamount is situated along a zone of weakness in the overriding plate's lithosphere. The fault trend that controlled the growth of the edifice has a northeast–southwest trend and intersects a northwest–southeast trend immediately south.

A primary feature of the summit of Yinazao Seamount is a fault scarp with a maximum throw of about 80 m that is colinear with the regional fault trend. The eastern half of the summit is shallower, and the overall morphology of the summit suggests a right-lateral motion on a fault with dip-slip to the northwest. The offset on the fault is apparently a combination of footwall uplift (eastern block) and downdrop of the hanging wall to the northwest (western block). This deformation may have directed the egress of rising fluids to the southwest edge of the summit area where a spring was located. Systematic variation in pore water composition from sediment piston cores collected from the research vessel (R/V) *Thomas G. Thompson* in 2003 confirmed the presence of fluid discharge at a rate of up to ~10 cm/y (Hulme et al., 2010). Discharge at rates of meters per year was identified from push cores collected in 2003 by the remotely operated vehicle (ROV) *Jason II* within a 50 m range of the piston core with the greatest fluid upwelling rate.

Coring on the flanks of Yinazao Seamount, as on those of the other two target mud volcanoes, was designed to recover some of the oldest serpentinite mudflow materials. We anticipated recovering matrix muds and rock clasts that would provide information regarding the lithology of these early erupted materials. Serpentinized peridotite clasts and other lithologies might reveal different decollement pressure, temperature, and compositional conditions from those that would be expected from the shallower (younger) periods as the shape of the forearc evolves, currently trending to the east. It was also expected that pore fluids would have interacted with seawater after lengthy exposure at the base of the seamount. Such interactions may affect microbial communities present in the subseafloor environment. Each of the five flank sites on these three seamounts is located on a multichannel seismic line that intersected either a region of the flank that was undisturbed by mass-wasting or that crossed the distal edge of a mudflow of particular interest.

Fantangisña Seamount (informally known as Celestial Seamount) is located about 62 km from the trench and about 14 km above the subducting Pacific plate (Figure **F1**; Table **T1**). This seamount lies on the northern edge of a prominent uplifted forearc block that trends northwest and its intersection with a northeast-trending lineament. The main feature of the summit is a slump on the northern flank. Several stages of slumps exist, based on nested headwalls with sharply defined features at 2000 and 1840 m water depth, for example.

No active seeps or chimneys were observed during the one ROV *Jason II* dive (J2-038) on Fantangisña Seamount in 2003. This dive started within the summit depression at the headwall of the 2000 m slump and headed up the southeastern slope to the summit rim. The only indication of active serpentinite processes is based on one piston core from the center of the summit depression. This core recovered 40 cm of serpentinite material; however, at the base of the core, concentrations of Mg and alkalinity (49.6 and 0.89 mmol/kg, respectively) in pore fluids were lower than bottom seawater values (53 and 2.4 mmol/kg, respectively). These data indicate a deep-sourced input close to the seafloor, consistent with slow, centimeters per year or less discharge of pore waters in excess of the sediment matrix.

Asùt Tesoru Seamount (informally called Big Blue Seamount) is a serpentinite mud volcano that lies about 72 km from the trench axis with the subducting slab approximately 18 km below its summit (Oakley et al., 2007, 2008) (Figure **F1**, Table **T1**). Asùt Tesoru Seamount is the farthest from the trench of the three seamounts targeted for coring. It is also the largest one on the Mariana forearc, with a diameter of ~50 km and over 2 km high. The major fault trend that controlled the growth of the edifice has a north-northeast trend and is crosscut by a fault trending north-northwest. Asùt Tesoru Seamount may have been active since the Eocene, based on analysis of two serpentine-bearing (~50% serpentine) sediment intervals immediately above Eocene basement recovered during Deep Sea Drilling Project (DSDP) Leg 60 at Site 459 (Despraires, 1981).

The summit region of Asùt Tesoru Seamount has a prominent mound at the intersection of the two fault trends. The summit mound is roughly circular and about 2 km in diameter and 300 m high. At its apex, it has three smaller circular mounds. One is centered at the middle of the 2 km wide mound and is about 150 m in diameter and 40 m high. The two other mounds are about 75 m in diameter and 20 m high. The two smaller mounds lie side by side

west of the larger mound and are both overlapped by it. An ROV transect of the larger mound was conducted in 2003 with the *Jason II* (J2-034 and J2-036) from west to east and explored farther to the northeast distant from the topographical high. The highest rate of fluid discharge occurred in the middle of the surveyed mound on the summit of the seamount.

South Chamorro Seamount is located about 78 km from the trench, with the subducting slab approximately 19 km below its summit; it was drilled during ODP Leg 195 (Figure **F1**; Table **T1**). This seamount is primarily composed of unconsolidated flows of serpentine mud with clasts consisting dominantly of serpentinized mantle peridotite but also includes blueschist fragments (Shipboard Scientific Party, 2002). The summit shows active fluid seepage of slab-derived fluids with megafaunal assemblages that include mussels, gastropods, worm tubes, and galatheid crabs (Fryer and Mottl, 1997). Subsurface microbes include archaea (Mottl et al., 2003; Curtis et al., 2013) and Bacteria (Takai et al., 2005). Even with evidence for fluid flow from a deep source (Hulme et al., 2010), temperatures measured in the uppermost 1 m at Site 1200 are between 2° and 3°C, which is just above the bottom water temperature of 1.7°C.

During Leg 195, a borehole observatory (CORK) was deployed. This original-style CORK included a 202.8 m long casing with a screened section from about 148.8 to 202.3 meters below seafloor (mbsf). This screened section provides a conduit for formation fluids at depth to exchange with fluids within the borehole. When the borehole is open at the seafloor, fluids naturally discharge (Wheat et al., 2008). However, the lack of latches to maintain formation pressure and the small diameter imposed by the original-style CORK limit the usefulness of this installation. The plan for Expedition 366 was to remove the CORK body, leaving the hole open for a future ROV deployment of a CORK-lite (Wheat et al., 2012).

Objectives

The four primary scientific goals outlined in the Expedition 366 *Scientific Prospectus* were to assess (1) mass transport processes in the Mariana forearc region, (2) spatial variability of slab-related fluids, (3) metamorphic and tectonic history and physical properties of the subduction zone, and (4) biological activity associated with deep-derived subduction zone material. To meet or address these goals, the specific objectives were to gain better insight into mass transport (fluids and solid materials) in the Mariana forearc region and its relationship to subduction zone tectonics and subseafloor biological processes. The sites chosen for drilling on the three target serpentinite mud volcanoes span different distances (thus depth to slab) from the Mariana Trench. Results from Expedition 366 will therefore complement previous drilling completed during ODP Legs 125 and 195. In addition, the long-term goal of the expedition was to establish borehole observatory sites at the summits of the three seamounts targeted for coring.

To meet the specific objectives for coring during Expedition 366, the operational plan was to (1) intersect mudflows of variable composition that mantled the flank of each edifice and, at the two that were known to be active, recover conduit muds from areas near active springs; (2) potentially date discrete mudflows paleontologically, should there be sediment layers between them; (3) determine variability in the composition of rock clasts in the mudflows; (4) investigate potential systematic variability in degree of serpentinization (possibly lower degrees at initiation of mud volcanism via conduit "throat clearing" or greater on the flanks where rock clasts may have reacted more fully with enclosing serpentinite muds and fluids); (5) examine transport conditions of muds and pore fluids; (6) provide a measure for the scale of potential flow characteristics (e.g., diffuse versus channelized); (7) determine the composition of fluid from depth; and (8) collect samples for the study of microbial/viral community interactions at depth and if possible near the underlying forearc sediment surface under a range of conditions.

The primary objective for establishing borehole observatories was to deploy three screened and cased boreholes that bisect hydrologic zones (aquifers), one at each of the three summit sites on Yinazao, Fantangisña, and Asùt Tesoro Seamounts. These boreholes, each sealed with cement at their base, would then serve as the foundation for a return mission with an ROV to emplace CORK-lites within the cased holes. CORK-lites would enable downhole monitoring, experimental capabilities, and collection of pristine deep-source fluids within a gas-tight sampling system for dissolved gas analyses. Given the original-style CORK at South Chamorro Seamount, the objective was to remove the CORK body so the borehole could be used for a range of experiment types and instrument sizes.

Coring results

Three serpentinite mud volcanoes were cored during Expedition 366 (Yinazao, Fantangisña, and Asùt Tesoro Seamounts). Cored materials were recovered from each of the summit and flank sites using a variety of coring technologies designed for maximum recovery, penetrating hard materials, or achieving a desired depth (Table **T2**). Thus, combined with data from Legs 125 and 195, the new data from Expedition 366 provide a continuum from relatively cool (~80°C) and shallow (~13 km) conditions at depth within the subduction channel closer to the trench to hot (~350°C) and deep (~19 km) conditions further from the trench (Table **T1**).

Materials recovered during drilling operations were analyzed using standard techniques commonly utilized on IODP expeditions. We present a summary of these data types and an initial interpretation organized by shipboard laboratory, providing an integrated vision of subsurface process based on data from each of the three cored sites. Each laboratory began the process of comparing and contrasting results from summit sites, which represent the most pristine materials in terms of transport from depth, and flank sites, where eruptive materials overlie previous deposits and have undergone alteration reactions made possible through diffusive exchange with overlying oxic bottom seawater. Ultimately, results from the various laboratories will be integrated to provide greater constraints for evaluating mass transport, temporal variability, metamorphic and tectonic history, and microbial mechanisms and activity.

Lithostratigraphy, petrology, and structure

Material recovered during Expedition 366 consists primarily of serpentinite mud containing lithic clasts derived from the underlying forearc crust and mantle and the subducting Pacific plate. A thin cover of pelagic sediment was found at many sites, whereas pelagic sediments and volcanic ash deposits were cored underlying serpentinite mud flows on the distal flanks of one of the three cored seamounts. The conceptual model for serpentinite mud volcanism processes within forearc/subduction complex is best described with a cross-section perpendicular to subduction (depicted schematically in Figure **F2**). Here, we describe in more detail the results from each site cored during Expedition 366.

The bulk of the material recovered in the cores is serpentinite mudflow matrix (Zone 1 in Figure **F2**). The matrix ranges from pale

green to dark blue-gray, except in the upper few meters of material recovered on the flanks of the seamount, where the serpentinite is typically oxidized to a yellow-orange color. The serpentinite mud consists largely of clay- to silt-sized serpentine grains plus accessory phases such as Fe oxide (magnetite and/or hematite), brucite, spinel, calcite, hydrogarnet, talc, tremolite, and chlorite. Secondary alteration minerals include sjogrenite group minerals, clays, aragonite, and gypsum. Authigenic aragonite, as single acicular needles or radiating clusters of acicular crystals, is common in the upper few tens of meters. Some serpentinite mud horizons appear to be reworked; these horizons may contain pelagic nannofossils, volcanic ash, and mineral fragments (e.g., clinopyroxene). Clast contents vary from <1 vol% to more than 35 vol% lithic clasts, with a mode of around 5 vol% lithic clasts.

Ultramafic clasts are the dominant clast type (Zone 4) and are mainly serpentinized harzburgite (<<5% clinopyroxene) with less common dunite and pyroxenite. The range in degree of serpentinization is broad, 30%–100% of the original material. Serpentinization is commonly pseudomorphic, and primary modes are inferred in most of the peridotites because the grain sizes for pyroxene (bastite) and spinel are largely unaffected. Primary textures were identified in most samples based on relict mineral phases or pyroxene-spinel relations. All dunites and most harzburgites (from Sites U1491, U1493–U1495, and U1497) are inferred to be porphyroclastic or coarse tabular primary textures with elongate, deformed olivine and enstatite, smaller strain-free neoblasts of olivine, as well as holly leaf–shaped interstitial spinel (e.g., Mercier and Nicolas, 1975; Lenoir et al., 2000). These textures imply that serpentinite materials have undergone solid-state deformation in the lithosphere at relatively low temperatures.

In contrast, harzburgites from Sites U1492 and U1498 are characterized by protogranular textures, with vermicular spinel-pyroxene clusters inferred to represent decompression breakdown of garnet (Smith, 1977; Bhanot et al., in press). The protogranular textures are overprinted by a subsequent texture formed in response to diffuse porous flow and reactive melt transport. Orthopyroxene has ragged lobate margins with sharp cusps that point into olivine grain boundaries (or former grain boundaries); some olivine grains have flat facets against orthopyroxene, signifying crystal growth faces in a melt; and olivine also occurs as euhedral to anhedral inclusions within larger orthopyroxene grains. Resorbed orthopyroxene sometimes has an oikocrystic appearance, with scattered fragments with the same optical orientation. Textures resembled postcumulus textures in cumulate rocks. These textures are inferred to be melt infiltration textures formed by reactive diffuse porous flow of a low-silica melt. This melt is undersaturated in orthopyroxene, which melted incongruently to form a silica-rich melt and new olivine. Because the delicate apices of interstitial pyroxene would likely be destroyed by solid-state flow in the lithosphere, we propose that this texture formed in the asthenosphere during melt production in response to subduction initiation.

No systematic changes of the serpentine textures were observed between the different sites (Zones 1–4 in Figures **F2**, **F3**). Serpentinized ultramafic rocks display mainly pseudomorphic mesh and bastite textures that replaced olivine and orthopyroxene, respectively. Such textures are likely composed of lizardite and chrysotile, but this assumption needs to be verified with postexpedition analyses. The mesh displays a pronounced blue color at Yinazao and Fantangisña Seamounts. Such coloration could be attributed to serpentine composition. Rare interpenetrating textures, which could correspond to the high pressure and temperature serpentine variety (antigorite), were mainly observed at Fantangisña and Asùt Tesoru Seamounts. Serpentinized ultramafic clasts are commonly crosscut by massive to fibrous veins of serpentine (chrysotile?), crystallizing into isolated networks of fractures, some of which are conjugate and some of which display crack-seal-like textures within the vein center. Although the cored serpentinite mud volcanoes are located at different distances from the Mariana Trench, the absence of a clear variation of serpentine textures in the ultramafic clasts suggests that the serpentinization process occurs continuously from the slab/mantle interface to the surface and that each mud volcano includes ultramafic clasts that were serpentinized at a range of depths (temperature and pressure). Late stages of serpentinite alteration were observed within each mud volcano, mainly corresponding to breccia consisting of fragments of serpentine minerals, serpentinites, and clay minerals cemented by carbonate. The fragmentation obliterated previous serpentine and mantle textures.

Crustal rocks derived from the underlying forearc crust and the subducting Pacific plate (Zones 3 and 6, respectively) were observed at several sites, but they form a major fraction of the recovered clasts at three sites: U1496 (Asùt Tesoru summit), U1497 (Fantangisña summit), and U1498 (Fantangisña flank). Low-grade metamorphosed sedimentary rocks and basalts were recovered from the summit site of Asùt Tesoru Seamount (Site U1496). These sedimentary clasts are fossiliferous cherty limestones. Mafic volcanic clasts are dolerites and augite-phyric vitrophyres, both with pink titanaugite.

Volcanic clasts from Fantangisña Seamount include forearc basalts (Zone 3), boninite and volcanic glass (boninitic), and greenstones and subgreenschist (prehnite-pumpellyite facies) metavolcanics (Zone 6). Metasediments from Sites U1497 and U1498 are characterized by recrystallization of calcareous and siliceous microfossils (Zone 5). The degree of recrystallization indicates low-grade metamorphic conditions. Metasedimentary and volcanic rocks are brecciated to varying degrees. Clasts from ultracataclastic shear zones with rounded clasts suggest deformation mechanisms along the plate boundary. Deformed sediment and volcanic rock clasts at these sites and at Site U1496 are consistent with a significant fraction of the material entrained by the Fantangisña and Asùt Tesoru Seamounts and derived from the subducting Pacific plate (Zones 5 and 6), whereas clasts of boninite and volcanic glass were more likely from the oceanic crust of the Philippine Sea plate (Zone 3).

The seamounts overlie pelagic sediment, which was sampled at Site U1498. This material is composed of volcanic ash, calcareous nannofossils (discoasters and coccoliths), foraminifers, radiolarians, and sponge spicules (Zone 2). The underlying volcanic ash establishes a maximum age for mud volcano activity or flank gravity sliding (Oakley et al., 2007). A similar pelagic sediment was recovered in the first cores from most flank sites; thus, paleontological analysis will help constrain the date of the most recent activity at each site.

Site U1491

Site U1491 is located on the flank of Yinazao Seamount near the base of a slight topographic valley. Mixed pelagic muds containing a variety of clastic materials were typically found at the tops of Holes U1491A (1.3 mbsf), U1491B (19.4 mbsf), and U1491C (34.2 mbsf) (Table **T2**). Beneath these pelagic sediments in Holes U1491B and U1491C, we recovered normally graded carbonate-dominated breccia-conglomerate sequences and serpentinite muds containing clasts of serpentinized ultramafic and occasionally carbonate (reef material?). The nature of the sediment units recovered in Holes U1491A–U1491C is consistent with the interpretation that these

units represent serpentinite mudflows, the deepest of which tapped a source of carbonate clasts and serpentinized ultramafic rocks that are likely far less matrix supported than observed previously. The source of the carbonate materials is possibly an underlying subducted Cretaceous seamount.

Site U1492

Site U1492 is located on the summit of Yinazao Seamount along the extension of an inferred normal fault. Holes U1492A, U1492B, U1492C, and U1492D were drilled to 38.3, 51.4, 139.1, and 228.8 mbsf, respectively; no materials were recovered from Hole U1492D (Table T2). Recovered materials from Holes U1492A–U1492C consist of an uppermost unit of red-brown pelagic mud with lithic clasts, generally <4 m thick, overlying a lower unit of blue-gray serpentinite pebbly mud containing 5%–10% lithic clasts of serpentinized ultramafic rock. The occurrence of pelagic mud at the summit of Yinazao Seamount is consistent with the observed sequence of predominantly serpentinite muds containing heavily serpentinized ultramafic clasts capped by a thin veneer of more oxidized, seawater-altered serpentinite muds and pelagic sediments. Hole U1492C has an intermediate unit of green serpentinite mud. Ultramafic clasts in the lowermost portions of the boreholes display the most extreme degrees of serpentinization, with continuous transition toward plastically deforming components. Conversely, ultramafic clasts in the brown to light green uppermost intervals retain their hardness and frequently exhibit milder degrees of alteration.

Sites U1493, U1494, and U1495

Sites U1493, U1494, and U1495 were drilled on a line from south to north on the south flank of Asùt Tesoru Seamount (Table T2). The deepest site (U1493; 3359 meters below sea level [mbsl]) is the closest to the distal southern edge of the edifice. Hole U1493A was drilled to 0.1 mbsf, and Hole U1493B was drilled to 32.6 mbsf. Site U1494, with only one hole (39 mbsf) at 2200 mbsl, is farther up the south slope, and Site U1495, at 1400 mbsl, is located just south of the summit mound.

Serpentinite muds are covered by brownish pelagic mud that contains volcanic ash, foraminifers, nannofossils, and minor diatoms and radiolarians. The thickness of the pelagic muds varies between sites, with approximately 80 cm in Hole U1493B, 0 cm in Hole U1494A (likely lost during mudline attempts), 6 cm in Hole U1495A, and 40 cm in Hole U1495B. Hole U1494A recovered an interval of mass flow between 6.9 and 8.78 mbsf that contains reworked serpentinite mud, volcanic ash, and brown muddy to silty fine sand with foraminifers that are assumed to derive from upslope sedimentary deposits. Holes U1495A (10.7 mbsf) and U1495B (10.8 mbsf) exposed a sequence of sandy silt with foraminifers and aragonite crystals overlying oxidized brownish and greenish gray serpentinite pebbly mud. The brownish gray serpentinite pebbly mud contains authigenic aragonite crystals and lithic clasts. The greenish gray serpentinite pebbly mud contains lithic clasts and occasional layers of matrix-supported breccia-conglomerate.

The three sites share a common stratigraphy that differs in detail with location. Uppermost recoveries consist of a layer of reddish oxidized sediments that include microfossil-bearing pelagic muds with volcanic ash near the surface and reddish yellow serpentinite muds. The thickness of pelagic sediments and microfossils generally decreases upslope. Beneath this layer, pale green serpentinite mudflows occur. These mudflows overlie several meters of dark blue to blue-gray serpentinite mud commonly intercalated with lighter green serpentinite mud.

Small clasts of mafic igneous rocks were recovered. These clasts resemble metabasalts, displaying green (chlorite and possibly epidote) and pale red (carbonate) layers. These clasts are either part of the subducted oceanic crust from the Pacific plate, altered by low-grade metamorphism and seafloor hydration processes, or from the crust of the overriding Mariana forearc area of the Philippine Sea plate.

Site U1496

Material from the summit of Asùt Tesoru Seamount (Holes U1496A [44.8 mbsf] and U1496B [36 mbsf]; Hole U1496C had no recovery) is characterized by a dominance of pale green serpentinite mud with a low proportion of lithic clasts compared to the seamount's flanks and other sites (Table T2). The pale green serpentinite mud is typically soupy or very soft due to high gas contents and often continued to out-gas days later. Dark blue serpentinite mud is uncommon, but when present it is characterized by higher clast counts. These characteristics are consistent with an active summit site that is currently producing high-pH water and abiotic hydrogen and methane.

Although less common than at other sites, hard rock clasts derived from the seamount summit mound provide important insights into the plumbing system of the mud volcano. Most common are ultramafic clasts, typically highly serpentinized harzburgites with less common dunite and orthopyroxenite. These materials likely derive from the underlying forearc mantle lithosphere.

We also recovered clasts of mafic metavolcanic and sedimentary rock. Sedimentary clasts included a fossiliferous, cherty limestone that may be pre-Eocene in age. Mafic metavolcanic clasts includ dolerites with pink titanaugite- and augite-phyric vitrophyres. The presence of pink clinopyroxene in these rocks suggests that their protoliths may have been alkali basalts. They are interpreted to be recycled material from subducted seamounts of the Pacific plate.

Site U1497

Four holes were drilled at Site U1497 on the summit of Fantangisña Seamount (Holes U1497A [34.2 mbsf] and U1497B [23.8 mbsf]; no recovery from Holes U1497C and U1497D) (Table T2). The occurrence of deformed sediments and volcanic rocks at this site suggests that a significant fraction of the material entrained by this mud volcano is derived from the subducting Pacific plate. In particular, the pink augite–bearing volcanic rocks implies mildly alkaline volcanic series in an ocean island seamount. In addition, the deformed sediments appeared to contain microfossils, such as radiolarians, that are representative of older (Mesozoic?) sediment from the Pacific plate. The presence of ultracataclasite, which requires severe brittle deformation, is unlikely to have occurred in sediments that were lying on top of the upper plate.

Mantle-derived harzburgites from Site U1497 are fully serpentinized but retain evidence of primary textures. They are characterized by pseudomorphs of orthopyroxene porphyroclasts that are highly elongated (in one case 4 mm × 0.4 mm), with kink folds and undulatory extinction. Spinel occurs in association with pyroxene and with subhedral to holly leaf shapes, 1–2 mm in size. We interpret these observations to indicate altered porphyroclastic textures, consistent with deformation at relatively low temperatures and moderate to high rates of strain. The (meta-) sediments are characterized by recrystallization of calcareous and siliceous micro-

fossils. The degree of recrystallization indicates low-grade metamorphic conditions. Both the metasedimentary and metavolcanic rocks are brecciated to varying degrees. Brecciation resulted in the development of fine-grained cataclasite to ultracataclasite domains. The very fine grained sediments (shales and sandstones) were partly transformed into ultracataclastic shear zones with rounded clasts. The very small grain size (<2 μm) within these shear zones indicates that the general deformation mechanism was ductile flow. Shear might have been localized along these shear zones. In general, brecciation (fracture) implies cataclastic deformation mechanisms (fracture and friction) at low-grade, moderate to high strain rates.

Site U1498

Site U1498 is located on the flank of Fantangisña Seamount. Hole U1498A (181.6 mbsf) is on the extreme southwestern flank, very close to the distal edge of the edifice and immediately downslope from a distinct break in slope of the lower flank (at 3507.5 mbsl) (Table **T2**). Hole U1498B (260 mbsf; 3296.0 mbsl) was ~700 m upslope northeast of Hole U1498A. Lithologies recovered at Site U1498A, with increasing depth in hole, include yellowish oxidized pelagic muds with pelagic microfossils; intercalated blue, green, and yellow-orange serpentinite mudflow matrix silts and sands; partially serpentinized ultramafic rocks (harzburgite and dunite); mafic metavolcanic rocks and boninites; and, at the bottom of the hole, nannofossil- and volcanic ash-rich sedimentary rocks (siltstones and fine sandstones). In addition, Hole U1498B returned a large (~2 m) compound clast of ultramafic rock, mafic metavolcanic rock, metalimestone, and metachert, likely originally within a serpentinite mud matrix, which was not recovered because the use of rotary coring likely washed out any existing matrix. All but the ultramafic rock was suspected to be part of a Cretaceous seamount.

The recovered clasts from Hole U1498B provide a particularly illuminating sequence of materials that deserves more detailed description. With increasing depth, the recovery includes (1) partially altered (to clay) serpentinized ultramafic rock clasts (stones and boulders), (2) serpentinite pebbly mud with pebbles of serpentinized ultramafics, (3) boulders of serpentinized ultramafics with numerous fractures filled with chrysotile, and (4) boulders of metabasite and cherty limestone and clasts of boninite and volcanic glass. These clasts and boulders were likely embedded within serpentinite pebbly mud (observed adhering to some of them), much of which was probably washed out during rotary coring. The mudflow matrix is well preserved in Sections 366-U1498B-7R-1 through 21R-1, 0–30 cm, with intermittent boulders. The most surprising recovery occurs in Core 21R. In Section 21R-1, 116 cm, there is a preserved and presumed inverted primary contact between a boulder of metabasite (35–116 cm; interpreted to be "igneous basement") and a boulder of cherty limestone (116–132 cm and continuing into Section 22R-1, 0–81 cm; interpreted to be "sedimentary cover," i.e., originally overlying the metabasite). The deformed cherty limestone appears to contain microfossils such as radiolarians that are common in older sediments from the Pacific plate. The texture and mineralogical composition of the metabasite (greenstone with chlorite and amphibole) and cherty limestone indicate low- to possibly medium-grade metamorphic overprint of these lithologies. These two boulders are clearly distinct from the volcanic rocks (boninites and forearc basalts) of the overriding Mariana forearc crust. The metabasite and limestones are consistent with a lower plate origin, and their paragenesis and position within the serpentinite mudflow matrix material suggests a dynamic overturning during exhumation. Furthermore, preserved cataclastic faults and extensional structures within these boulders (high-angle normal faults and extensional veins) may be related to (1) shearing within the subduction channel and bending of the lower plate during subduction, (2) incorporation and vertical tectonism of intact guyot masses into the forearc region, or (3) faulting during the early stages of exhumation. The presence of ultracataclasite in the cherty limestone boulder requires severe brittle deformation that would not likely occur in sediment from the overriding forearc crust. At the base of Section 22R-CC, 81–93 cm, is a serpentinite mudflow matrix that continues to Section 23R-1, 12 cm. A boulder of greenstone with numerous fractures infilled with white secondary precipitate was observed in Section 23R-1, 12–81 cm. At about Section 24R-1, 9 cm, we recovered a contact between serpentinite mud matrix containing serpentinized ultramafic rock and dark-gray, pelagic, vitric silt that contains microfossils. Thus we achieved our goal of penetrating into the sediment that predates serpentinite flows at this site. Beginning at Section 27R-1, 13 cm, we recovered intercalated pelagic, light tan to medium brown layers of pelagic, silty clay that persisted to the end of the hole.

Sediment and rock chemistry

A selection of representative serpentinites, sediments, and rocks recovered during Expedition 366 were analyzed with the new portable X-ray fluorescence spectrometer (pXRF). On the basis of these and visual results, a subset of materials was powdered for a suite of ship- and shore-based analyses (Table **T3**). In addition, a thin section was located next to each of the powered rock samples. At sea, powered samples were analyzed using standard inductively coupled plasma–atomic emission spectroscopy (ICP-AES) techniques to measure concentrations of Ni, Cr, Sr, Ba, Sc, V, and Zr, and the pXRF was used to determine concentrations of Fe, Ca, Mn, Ni, Cr, Zn, and Sr (Table **T4**).

Recovered serpentinites are largely uniform in composition, with serpentinized ultramafic rocks and serpentinite muds spanning a limited range in SiO_2, MgO, and Fe_2O_3 compositions (Figure **F4**). No significant site-to-site or seamount-to-seamount variability was evident in these major elements or in the variations in Al_2O_3, which range from 0.1 to 1.7 wt% with a mean value of ≈0.6 wt% (Table **T3**). This range is similar to the ranges reported by Savov et al. (2005a, 2005b, 2007) for serpentinized ultramafic clasts from Conical Seamount and for mudflow matrix and clasts from South Chamorro Seamount.

Fluid-immobile minor and trace elements Ni, Cr, Zn, V, and Sc show no clear distinctions from site to site or seamount to seamount in the serpentinized ultramafic rocks (Figure **F5**). V, Sc, Mn, and Zn show regular patterns of variation; these elements appear not to be redistributed by fluid-rock exchanges associated with serpentinization. TiO_2 variations in serpentinites differ from those of the other immobile elements in that there may be site-related variability, with higher values evident for Site U1496 samples. However, Ti concentrations are close to the limits of detection using the shipboard ICP-AES, with only a fraction of our samples yielding detectable readings. It is equally possible that this small number of higher values were analytical artifacts.

Major and trace elements that are sensitive to redistribution by fluid-rock exchange processes with ultramafic rocks show more variable patterns. CaO concentrations show considerable variability, ranging from <0.01 to >10 wt% across a limited range in MgO values (Figure **F6**). Samples analyzed from all three seamounts include rocks with both CaO ≥ 10 wt% and high MgO, suggestive of ultramafic cumulate bulk compositions for some of the ser-

pentinized ultramafic rocks. A plot of Na_2O versus MgO (Figure **F6**) shows an evident distinction between the serpentinized ultramafic clasts, which have Na_2O values of >0.4 wt%, and the serpentinite muds, which range as high as 2.0 wt% Na_2O. Seamount-to-seamount variations are evident; serpentinite muds from the Asùt Tesoru summit site (U1496) have higher Na_2O concentrations than those from the summit of Yinazao Seamount (Site U1492) or Fantangisña Seamount (Site U1497). Pore fluids at the Asùt Tesoru summit are markedly higher in Na than those from the summits of Fantangisña or Yinazao Seamounts. Thus, the high Na_2O in Asùt Tesoru muds may reflect equilibration with these Na-enriched pore fluids.

Sr concentrations in serpentinites are highly variable, ranging from <5 to >6000 ppm. As with Na, the serpentinized ultramafic clasts are lower, all with ≤100 ppm Sr, relative to the serpentinite muds (100–6000+ ppm; mean ≈ 600 ppm). In addition, there are clear seamount-to-seamount differences in the serpentinite composition of the muds, likely related to equilibrium with their associated pore fluids. Yinazao Seamount muds (Site U1492; pore fluids > 700 µM) are markedly higher in Sr than those from Asùt Tesoru Seamount (Site U1496; pore fluids ≤ 10 µM). The highest Sr and Ca in sediment samples were found in near-surface cores and relate to the presence of authigenic aragonite and/or gypsum.

A small but unique number of metamorphosed mafic volcanic and crustal rocks (sedimentary breccias, metamorphosed basalts, and boninites) were recovered, primarily from the summits of Asùt Tesoru Seamount (Site U1496) and Fantangisña Seamount (Sites U1497 and U1498) (Tables **T3**, **T4**). These metabasalts show elevated concentrations of TiO_2 (1.6%–3.3%) and K_2O (2.7%–6.7%) and range from 16 to 18.6 wt% in Al_2O_3, with highly variable MgO (2.5%–11.3%) and Na_2O (0.8%–3.5%) (Figure **F7**). Analyzed samples have Ni concentrations of ~55 ppm, high V and Sc concentrations (up to 280 and 28 ppm, respectively) (Figure **F5**), Sr concentrations between 54 and 236 ppm (Figure **F6**), Ba concentrations up to 88 ppm, and Zr concentrations between ~240 and 470 ppm. There is evidence for within-clast heterogeneity; samples from each of the two core sections characterized by mafic clasts (Sections 366-U1496B-8X-CC and 10F-2) show considerable variability in a number of immobile and mobile elements. Plotted on the Shervais (1982) V-Ti tectonic classification diagram, these rocks are similar to those from the intraplate/alkali basalt field (Figure **F5**).

The metamorphosed mafic rocks resemble a subset of (1) samples recovered from dredges along a wall of a forearc graben north of the sites drilled during Expedition 366 (Johnson and Fryer, 1990) and (2) trachybasalts recovered from the western Pacific immediately outboard of the Mariana Trench (**http://www.iedadata.org**). These mafic rocks do not resemble the forearc tholeiite and boninite lavas that were known to comprise the volcanic crust of the outer Mariana forearc (e.g., Reagan et al., 2010). Thus, the most likely origin for these rocks is the downgoing Pacific plate, where seamounts that expose alkalic lavas are currently subducting.

Pore water geochemistry

Studies of pore fluid geochemistry from summit sites cored during Expedition 366 focused on collecting end-member compositional information, thus improving our overall understanding of the deep-sourced processes. In contrast, studies of pore fluids from the flanks of the three cored seamounts focused on elucidating compositional changes of pore fluids with time in the context of water-rock reactions, diffusive exchange with seawater, microbial activity, and processes associated with pelagic sediments that underlie serpentinite mud volcanoes in the Mariana forearc.

Measured dissolved gases H_2, CH_4, and C_2H_6 provide important insights into the physical and chemical conditions of the deep source. High concentrations of dissolved H_2, CH_4, and C_2H_6 were measured in samples from the summit of Asùt Tesoru Seamount, and comparatively low but significant levels were detected at Yinazao Seamount summit and flank sites. Variability in gas compositions among the three seamounts indicate differences in serpentinization and fluid migration process. Dissolved H_2 and CH_4 (Figure **F8A**) show two groupings broadly consistent with thermodynamic estimates of serpentinization-driven H_2 production (McCollom and Bach, 2009) and subsequent abiotic (Fischer-Tropsch Type) CH_4 production.

Plots of methane versus ethane data from Asùt Tesoru, Conical, and South Chamorro Seamounts reveal linear trends (Figure **F8B**). Data from Asùt Tesoru Seamount are consistent with trends from South Chamorro and Conical Seamounts. These trends may reflect different methane consumption rates and/or methane production rates of subseafloor microbial communities, likely associated with habitability, abundance, and function. Both trends converge at a potential end-member composition (CH_4 = 60–100 mM, C_2H_6 = 600–1000 µM, and C_1/C_2 ratio = 100–150) that may represent the hydrocarbon values predominantly produced by abiotic (Fisher-Tropsch Type) synthesis processes at depth.

The chemical composition of deep-sourced pore fluids was assessed along the continuum from shallow to deep source and from closest to farthest from the trench (Yinazao, Fantangisña, Asùt Tesoru, South Chamorro, and Conical Seamounts) (Table **T1**; Figure **F9**). Fluids from the summits of Yinazao and, to a lesser extent, Fantangisña Seamounts show elevated Ca and Sr and low to extremely low K, Na, Cl, SO_4, B, and Na/Cl concentrations relative to bottom seawater. In contrast, fluids that upwelled at the summit of Asùt Tesoru seamount are similar in composition to those from South Chamorro and Conical Seamounts, with extremely high pH values (up to 12.4), Ca and Sr depletions, and marked enrichments in carbonate alkalinity, dissolved inorganic carbon (DIC), dissolved organic carbon (DOC), NH_4, Na, K, Na/Cl, and B. Na concentrations are higher at Asùt Tesoru than any of these five seamounts (Figure **F9**; see discussion below).

We mapped changes in chemical composition of pore fluids across the Mariana forearc in relation to subduction-related prograde diagenetic and metamorphic reactions that may trigger fluid and elemental releases (Figures **F10**, **F11**). Processes that occurred early (shallow) within the subduction system (i.e., Yinazao and Fantangisña Seamounts) were likely dominated by diagenesis and opal dehydration, whereas later processes (deeper) (i.e., Asùt Tesoru Seamount) included decarbonation and clay mineral decomposition (Fryer, Pearce, Stokking, et al., 1990; Haggerty, 1991; Haggerty and Chaudhuri, 1992; Haggerty and Fisher, 1992; Mottl, 1992; Mottl and Alt, 1992; Fryer et al., 1998; Mottl et al., 2003, 2004; Hulme et al., 2010; Wheat et al., 2008, 2010). Higher DIC at greater depths-to-slab is likely linked to carbonate decomposition within the slab. DIC reacting with H_2 from serpentinization could produce CH_4, light alkanes, or short-chained organic molecules (e.g., acetate and formate). Ca and Sr were sequestered from the fluids by carbonate precipitation (the lack of calcite in core samples from Asùt Tesoru Seamount suggests this reaction occurred slightly closer to the trench, which would exhaust Ca with continued CO_3^{2-} production). Although Asùt Tesoru Seamount's pore fluids are broadly similar to

those studied at South Chamorro and Conical Seamounts, they are nonetheless distinct, with much higher Na and Cl concentrations and 3–4 times lower B contents. These differences likely reflect the lowest pressure-temperature (P-T) prograde metamorphic mineralogical reactions, impacting slab sediments and saponites that result in fluid release (Figure **F11**).

This slab signal is overprinted by low-temperature peridotite-seawater reactions and by microbial interaction with fluids, particularly near the seafloor (Mottl et al., 2003; Takai et al., 2005; Curtis et al., 2013) and on the flanks of the seamounts. Initial pore fluid results from five flank sites cored during Expedition 366 indicate that the fluids are mixtures of slab-derived fluids that have undergone various degrees of alteration with serpentinite materials in the mud flows and exchange with overlying seawater.

Microbiology

Sample recovery

Microbiology sampling during Expedition 366 focused on exploring the limits of microbial life and viral components in serpentinite mudflow habitats across multiple depths using cultivation-based and cultivation-independent molecular biological approaches and microscopy. Sampling efforts targeted both near-surface and deeper whole-round cores, especially if there was evidence of a transition across gradients of microbiologically affecting compounds and gases (e.g., hydrogen, methane, hydrogen sulfide, and sulfate). Two 20 cm long whole-round samples were collected at each sampled depth for general microbial analyses (Table **T5**). Additional whole-round samples were collected for individual investigations. Samples were collected within the context of tracer studies to assess potential contamination resulting from the drilling and sample recovery processes.

Microbiological samples will be analyzed on shore using an array of microbial community–level interrogation techniques. Samples were fixed for total cell counts to quantify microbial biomass. Other samples were maintained at 4°C for multiple cultivation techniques (including fluorescence-activated cell sorter [FACS] high-throughput media screening and detection of adaptation to physical parameters such as pressure tolerance). Other samples were flash-frozen at −80°C for molecular analyses, including small-subunit (SSU) ribosomal gene amplicon sequencing (to address community structure in greater detail), functional gene detection and quantification through real-time quantitative polymerase chain reaction (qPCR), and single-cell genomics (to specifically address individual cell contributions). In addition, metagenomics of the entire microbial community and metatranscriptomics of the most highly expressed genes will be used to establish metabolic potential and deeper ecological and evolutionary relationships. Lastly, samples were preserved for enumerating viral counts and assessing viral diversity.

Contamination testing

Perfluoromethylcyclohexane (PMCH) was used at the first two sites (U1491 and U1492) and the last site (U1498), whereas perfluoromethyldecalin (PFMD) was used at the remaining sites (U1493–U1497). This split was partially due to tracer availability and partially to our ability to establish proper protocols for both perfluorocarbon tracers (PFTs). Data obtained from PMCH measurements show relatively clean (uncontaminated) drilling by advanced piston corer (APC) and half-length APC (HLAPC) operations at Site U1492. This analysis, however, indicates disturbance in cores and drill fluid intrusion at Site U1498, which was drilled using a rotary core barrel (RCB) technique. Generally, drill fluid intrusion into samples was higher at sites where drilling became difficult and required the use of either extended core barrel (XCB) or RCB drilling.

Unfortunately, analysis of the PFMD data does not provide a distinct indication of contamination compared to results using the PMCH tracer. PFMD is a relatively new method for contamination tracing, and the results from this expedition strongly reinforce the need for further method development if it is to be used when coring sediment.

Shipboard DNA extraction and qPCR

Shipboard DNA extraction from serpentinite mud samples was unsuccessful using a standard qPCR protocol (e.g., Lever et al., 2015). Additional analysis shows high adsorption of DNA to serpentinite minerals; thus, improvements in DNA extraction protocols in terms of adsorption prevention will be necessary for further DNA extractions. Performing qPCRs on board the R/V *JOIDES Resolution* is feasible and can expand the range of available shipboard analyses for future expeditions.

Physical properties

Among the eight sites that were drilled during Expedition 366, the physical properties obtained at the two summit sites at Yinazao and Asùt Tesoru Seamounts (U1492 and U1496, respectively) are distinct. Physical property values are usually associated with consolidation and compaction of sedimentary deposits (e.g., bulk density, porosity, thermal conductivity, and shear strength); however, data from the two summit sites, at the active spring areas observed from the ROV *Jason II*, indicate that serpentinite muds at these sites were subject to different processes than those at the other sites, which experienced "typical" consolidation.

For example, the porosity data collected during Expedition 366 followed two trends (Figure **F12**). One trend was defined by data from summit Sites U1492 and U1496 and ODP Site 780. At each of these sites, porosity decreases with depth from seafloor values of 60%–70% to values of 45%–55% at 120 mbsf. An exponential trend was fit to the Site U1492 data, resulting in an Athy's coefficient (Athy, 1930) of 0.36, indicating that this summit site is slightly underconsolidated (Bekins and Dreiss, 1992). Both sites (U1492 and U1496) are located in areas of fluid discharge where discharge rates exceed 10 cm/y (Hulme et al., 2010). These sites targeted our best estimate for the location of the current conduit for fluid and material flow from depth. A slight compaction effect is suggested in Holes U1492A and U1492B by the overall increasing trend in gamma ray attenuation (GRA) density with depth, whereas Hole U1492C, the closest one to the presumptive conduit, has lower GRA values and a rather constant trend to the bottom of the hole (~130 mbsf) (Figure **F13**). Likewise, consolidation and compaction trends with depth in Hole U1496A at Asùt Tesoru Seamount show a slight increase of bulk density, whereas no such trend was observed in Hole U1496B. The rather constant GRA bulk density and porosity values observed in Holes U1492C and U1496B, both located less than 20 m from the presumptive conduit area, are jointly influenced by overpressured fluids localized in the immediate (~20 m) region of the central conduit system, which minimized the compaction of serpentinite mud deposits at these holes. In contrast, GRA density increases in Holes U1492A, U1492B, and U1496A suggest this overpressure effect associated with the conduit system is not effective 50 to 100 m from the area with the most active fluid discharge. A width of less than ~100 m for the active conduit at Yinazao and Asùt Tesoru Seamounts is consistent with conduit diameters, which are

considerably smaller than the size of the mud volcanoes themselves and those described for other mud volcanoes (Krastel et al., 2003).

In contrast, there is a greater decrease in porosity with depth at the other sites (mostly flank sites) to porosity values less than 30% at only 40 mbsf. The Athy coefficient fit at Site U1494, for example, is 17.3—unreasonably high for a compaction trend. Below 40 mbsf, porosity values stabilize and remain fairly constant with depth. Such low porosities (and high Athy coefficients) are suggestive of processes other than compaction being responsible for the observed data.

Although similar, there are slight peculiarities in data from the other sites. Even the two sites located on the edge of seamount summits, Sites U1495 and U1497, show behavior more typical of flank sites. The porosity trend at Site U1495 resembles other flank sites but is more extreme, decreasing from 57% to 36% at only 4 mbsf.

The third summit site (Site U1497 on Fantangisña Seamount) is distinct from the other two summit sites. The porosity trend with depth is comparable to those described for the other flank sites (Figure **F12**). These trends suggest that either the mud volcano has not been active recently or subsurface flow in this area was either diffuse, compartmentalized, and not necessarily vertical or was following trends in local faults associated with the slump features at the summit.

Downhole measurements

Temperature measurements using the advanced piston corer temperature tool (APCT-3) were attempted 14 times, resulting in 11 records that were used to estimate formation temperatures. These estimates were combined with measured seafloor temperatures and thermal conductivities from collected cores to calculate heat flow for the three summit sites and two of the flank sites (Table **T6**). The summit heat flow values range from 16.8 to 17.8 mW/m^2, whereas the two flank sites range from 30.5 to 31.9 mW/m^2 (Figure **F14**). These values and differences are consistent with data from the South Chamorro Seamount summit, which average 15 mW/m^2 in ODP Holes 1200A and 1200E (Shipboard Scientific Party, 2002), and those collected on the flanks of Conical Seamount at DSDP Sites 458 and 459 (Uyeda and Horai, 1981).

Wireline logging was conducted in Hole U1498B after penetrating to 260 mbsf. The triple combo tool string was used to measure magnetic susceptibility, natural gamma radiation (NGR), electrical resistivity, borehole diameter, and temperature of borehole fluids. The downhole logging data show excellent agreement with the shipboard data. The NGR data are consistent with 9 m of pelagic sediment at the sediment/water interface that was not recovered during coring operations and registered the cherty limestone and metabasalt units. Two possible layers of pelagic sediments may be present at 118 and 137 mbsf intercalated within the serpentinite (e.g., pale streaks in intervals 366-U1498B-13R-4, 21–25 cm, and 15R-3, 6–10 cm). Here, peaks in NGR values are at similar levels to the Unit I, presumable ash-rich pelagic sediments that are thought to exist in the upper 9 m of Hole U1498A. Additional evidence for layers of pelagic sediment is the lack of evidence in the resistivity data for clasts. The resistivity data were useful for detecting large clasts.

Paleomagnetism

The new 2G Enterprises superconducting rock magnetometer (SRM; liquid helium free) was installed at the start of Expedition 366. Paleomagnetic analyses of archive halves and representative discrete samples were performed. The natural remanent magnetization (NRM) of almost all section halves was measured at 5 cm intervals after 0, 5, 10, 15, and 20 mT alternating field (AF) demagnetization steps. The use of principal component analyses (PCA) provided consistent NRM inclination and declination values between section halves and discrete samples.

A pervasive vertical magnetic overprint was imparted to the cores, likely by the drilling process. In some cases, overprinting was largely demagnetized by AF demagnetization in peak fields of 5 mT; in many intervals, however, enough of the overprint remains after the 20 mT demagnetization step that inclination values remain anomalously high. The axial dipole inclination was expected to be between 29.5° and 33.2° at the latitude (15.8°–18.1°N) of coring operations. We searched for paleomagnetic reversals for magnetostratigraphic dating in the volcanic ash-rich pelagic sediments that overlie the serpentinite muds, but no clear reversals were found. In some cores, a particularly high intensity overprint was observed between 3 and 5 m above the base of the core, for example, Cores 366-U1492C-5F and 8F (Figure **F15**).

Magnetic susceptibility levels are generally high, reflecting the high concentrations of magnetic minerals, particularly magnetite, in the cores. Magnetite was of interest because it was produced during serpentinization reactions, to a greater or lesser extent depending on the iron content of the initial minerals. Magnetic susceptibility is higher at the Asùt Tesoru sites, averaging over 1000 SI, compared to the other two mud volcanoes (Figure **F15**). There is some local correlation between magnetic susceptibility levels and the color of the serpentinite mud, but no correlation across all of the sites. In Hole U1496A, for example, the darker mud between 26 and 27 mbsf has five times lower susceptibility than the surrounding pale green serpentinite mud, whereas in Hole U1493, the pale green serpentinite mud at 20–23 mbsf has much lower susceptibility than the blue-gray mud above and below it.

Magnetic intensities are high, given the high concentrations of magnetic minerals, but there is an unexpectedly large range of intensity values (Figure **F15**). At Site U1496, the paleomagnetic intensity is relatively low and correlates with magnetic susceptibility, as expected from a consistent lithology and magnetization process. At other sites, however, magnetic intensity is relatively high compared to magnetic susceptibility, and the correlation between the two is less clear, perhaps due to the difficulty in demagnetizing the variable overprint in many of these cores. NRM intensity generally ranges from 1.0×10^{-3} to 1.0 A/m, reaching maximum values of 10 A/m in Hole U1494A in a dark bluish gray serpentinite pebbly mud. Generally, ultramafic rock clasts present relatively high values of both magnetization and bulk magnetic susceptibility in discrete samples.

Cased borehole operations and results

Each of the four serpentinite mud volcanoes visited during Expedition 366 (Yinazao, Fantangisña, Asùt Tesoro, and South Chamorro Seamounts) included a borehole operational component. The goal was to deploy an infrastructure that intersected an active hydrologic flow of deep-sourced fluid along a continuum of conditions across the forearc. These boreholes include screened sections to allow formation fluids to enter and are designed for future deployments of CORK-lites (Wheat et al., 2012). This construct will enable the community to use the boreholes for scientific endeavors, including but not limited to monitoring physical and chemical changes, in situ passive experimentation, and manipulative experiments to address a range of potential scientific questions that center on geophysical, geochemical, and/or microbial studies.

A CORK-lite has a modular design that includes multiple ports for experiments and sensors inside or outside of the CORK body and for large-diameter (25 cm) experiments and sensors to be deployed within the boreholes, which can be either sealed or allowed to discharge.

South Chamorro Seamount (Site 1200)

Given the limitations of the original-style CORK that was deployed at Site 1200 during Leg 195, the plan was to remove the CORK body, thus leaving the hole open for a future ROV deployment of a CORK-lite (Wheat et al., 2012). While attempting to remove the CORK body, the latch rods failed to remove the portion of the CORK that latches into the casing hanger, forming a seal and focusing discharge up a steel pipe that contains the seal sleeve. This steel pipe parted above the seal sleeve. However, the CORK is likely sealed with access to the underlying casing via a portion of a PVC insert that was deployed in 2009, providing a conduit for future sampling activities. The recovered CORK body included white and reddish material on the outside that was collected for microbial and mineralogical analyses. About seven limpets also were recovered from the CORK body and preserved for shore-based identification.

Yinazao (Site U1492), Fantangisña (Site U1497), and Asùt Tesoro (Site U1496) Seamounts

A casing string was deployed after an initial hole was drilled into the summit region at Yinazao, Fantangisña, and Asùt Tesoro Seamounts. The casing string included at least three joints of screened casing, placing the screened casing as deep as possible and well below the near-surface microbial "transition" layer (e.g., Mottl et al., 2003). Difficulties experienced during the deployment of the first casing string changed the depth and design of the second and third deployments.

The initial borehole casing string was deployed at Site U1492. This casing string was 211 m long with a screened section at 153–199 mbsf. The other two casing strings were shorter (~110 m long) with screened sections at ~35–70 mbsf. A cement plug was deployed at the base of each of the three casing strings because of a failure during the deployment of a mechanical bridge plug at Site U1492; however, later operations did break the bridge plug free so the base of the casing string could be cemented. These cementing operations were important because serpentinite material flowed into the base of the casing string at Site U1496 within hours of landing the casing within the casing hanger, filling the bottom 7 m of the open cased hole. We returned to two (Sites U1496 and U1497) of the three boreholes to check the status of the cement and collect a water sample with the water-sampling temperature probe (WSTP) within these two boreholes. We did not have time to return to the cased borehole at Site U1492 after cementing operations.

The cement plug was reached at both sites (U1496 and U1497) several days after cementing operations. The cement was in place as planned and likely sealed the boreholes from intruding material. Water samples were collected from the middle of the upper screened casing joint at both sites. Analysis of this water indicates a mixture of seawater and formation fluid. The Site U1496 sample includes the highest dissolved gas measurements made during the expedition, highlighting the importance of sampling formation fluids directly and without the artifacts induced by the coring and sample handling process.

Each of the three new boreholes tapped an active hydrologic zone with formation fluids that discharge into the casing and vent at the seafloor. By deploying a CORK-lite with an ROV, the community will be able to collect pristine fluids (especially dissolved gases) that are unaffected by sampling artifacts. The community also will be able to collect and/or filter tens to thousands of liters of formation fluid for chemical, microbial, and viral analyses, volumes that are not possible to obtain during standard IODP coring operations. The deployment of CORK-lites also opens the cased boreholes to a range of sensors, samplers, and experiments that will allow scientists to build a network of experiments, monitoring, and manipulations at the seafloor or within the borehole and with the boreholes sealed or open to discharge.

Preliminary scientific assessment

Expedition 366 successfully cored the flanks and summit regions of three Mariana forearc serpentinite mud volcanoes, each located at varying depth to the subducting Pacific plate, to characterize processes associated with the formation and activity of these mud volcanoes. The expedition was designed to examine subduction-related processes in terms of the relationship between geochemical cycling, seismicity, and deep biosphere activity in subduction zones and suprasubduction zone lithosphere. The intent of the expedition was to address how these processes vary spatially along the strike of the Mariana system and with depth to the subduction channel (~13 to 18 km below). The results from this expedition complement those from previous Legs 125 and 195 at two other serpentinite mud volcanoes, Conical and South Chamorro Seamounts, both further from the trench than the three cored during Expedition 366.

Previous drilling during Leg 125 used rotary coring, and poor recovery failed to provide much of the mudflow matrix in which the rock clasts were entrained. Leg 195 used APC/XCB coring and recovered many thin mudflows, some with more than 100% recovery, because the matrix contained gases that expanded upon recovery. During Expedition 366, all three coring systems were used, each for a specific purpose. Drilling results during Legs 125 and 195 proved that the mudflows contain, in part, materials from the subduction channel below the edifices. Expedition 366 recovered a greater diversity of subduction channel material from closer to the Mariana Trench, thus from shallower depth-to-slab, than material recovered in the two previous legs. Rock clasts and matrix muds from the serpentinite flows recovered during Expedition 366 provide a far better view of the regional processes that have affected the forearc. Furthermore, the cased holes with screened sections that were drilled into the summit regions of these three mud volcanoes now constitute the first regional laboratory for monitoring subduction-related phenomena in the trench-proximal region of a nonaccretionary, intraoceanic, convergent plate margin.

We achieved or will achieve with shore-based analyses all four of the overarching scientific goals outlined in the Expedition 366 *Scientific Prospectus*. These goals were to assess (1) mass transport processes in the Mariana forearc region, (2) spatial variability of slab-related fluids, (3) metamorphic and tectonic history and physical properties of the subduction zone, and (4) biological activity associated with deep-derived subduction zone material. Associated with these four scientific goals are nine specific objectives, described below.

1. *Core mudflows on the flanks of each mud volcano and recover conduit muds from areas near active springs on the summit of each mud volcano.*

This objective allowed us to address both construction history and transport processes. We recovered serpentinite mudflows with

variable characteristics on the flank of each edifice from Sites U1491 (Yinazao Seamount), U1493, U1494, U1495 (Asùt Tesoru Seamount), and U1498 (Fantangisña Seamount). The serpentinite mudflow matrix varies in color with depth, and although it was distinctly disturbed by flow-in during APC and XCB coring, it does preserve discrete horizons of clast content and matrix constituents. The cause of the color change in the serpentinite muds is not obvious and will become the focus of several proposed shore-based studies. Although we were without X-ray diffraction (XRD) or X-ray fluorescence (XRF) instruments during Expedition 366, samples analyzed with a pXRF and ICP-AES showed essentially no difference in the major elements between the compositions of the serpentinized rock clasts and muds from seamount to seamount, except for specific major and trace elements that are sensitive to redistribution by fluid-rock exchange processes. These elements showed more variable patterns in the matrix and fluid data, indicating a regional consistency with depth-to-slab. Expedition 366 results confirm the broad interpretation of gravity core, piston core, and submersible/ROV push core work over the past decade that revealed a regional gradient in terms of change in slab-related fluids with depth to the subduction channel recorded by the fluids rising in active springs in serpentinite mud volcanoes. The enhancement of this finding as a result of Expedition 366 was that the source of most of the fluids is initially prehnite-pumpellyite facies dehydration followed by greenschist alteration and lastly blueschist dehydration and mobilization of fluid mobile elements. For example, boron and potassium data show drastic increases in the concentration in muds and fluids with distance from the trench. There remain questions regarding the eruptive processes. Such questions would be better addressed through monitoring. For example, how variable were the volumes of erupted materials, and what controls the eruptive cycle? The planned CORK-lite installations at the cased boreholes will be instrumental in addressing temporal-related questions.

2. *Date discrete mudflows paleontologically, should there be sediment layers between them.*

Dating discrete layers will help to better understand the episodicity of the eruptions and how differences among episodes may affect transport processes. Dating will be possible as a consequence of recovering pelagic sediment overlying flank serpentinite mudflows and because we were able to penetrate the underlying forearc sediments at two of the holes on Fantangisña Seamount's flank. We recovered interlayered mudflows of clay-sized serpentinite mud of a wide variety of oxidized and unoxidized material, as well as interlayered pelagic sediments on the distal edges of Fantangisña Seamount. Very few rock clasts were found in these mudflows. Also, beneath the serpentinite on Fantangisña Seamount, we recovered ash-rich sediment with abundant microfossils. Biostratigraphic ages for the recovered sediments will be determined on shore. The recovery of this material is reminiscent of that in the deepest sediment interval (near Eocene igneous basement) in Hole 459 (Leg 60), which is located south of Asùt Tesoro Seamount (Despraires, 1982).

3. *Determine variability in the composition of rock clasts in the mudflows.*

The anticipated discovery of subduction channel physical and compositional properties was realized through the recovery of numerous rock clasts. We discovered striking variability in the lithology of the clasts within the mudflows, and the results of shipboard observations and analysis show that all five of the serpentinite seamounts cored to date (including Leg 125 and 195 cores) contain materials from the subducted slab. The fact that all of these mud volcanoes tapped slab-derived fluids and erupt rock clasts from the subduction channel confirms that these edifices are indeed natural windows to slab processes. The range of recovered material from Expedition 366 is particularly illuminating because we recovered coralline material and metavolcanics with alkalic provenance, as well as compositions consistent with ocean island basalts and shallow intrusives. These lithologies indicate a source from subducted Pacific plate seamounts. Also collected were clasts that span the entire range of lithospheric compositions known to have formed in the suprasubduction-zone region of the Mariana forearc. Thus, Expedition 366 results also confirm that serpentinite mud volcanoes erupt the entire suite of rock materials that represent the subsurface architecture of the Mariana arc. The fact that the mud volcanoes occur exclusively in association with forearc scarps suggests that vertical tectonism of the forearc is the rule rather than the exception.

4. *Study potential systematic variability in the degree of serpentinization of rock clasts and distinguish the characteristics of the mudflow matrix on the flanks from those in the summit conduit regions.*

Coring on the flanks of the edifices revealed for the first time that there is systematic increase in the degree of serpentinization of rock clasts and of secondary mineralization of the mudflow matrix with increasing depth down the flanks of the mud volcanoes. Most ultramafic clasts recovered from the flanks reacted to a greater extent with muds that are generally 100% serpentinized. Furthermore, individual serpentinized rock clasts are soft enough to indent with a fingernail. Reaction of the clasts with the matrix muds is evident where halos surround clasts and darken the adjacent mud. The degree of serpentinization in ultramafic clasts is variable in the summit regions, where episodicity of activity in the conduits of these edifices may cause pulsing, presumably on various timescales, of the mud matrix and fluids and may refresh the throat with new, and less reacted materials.

5. *Examine transport conditions of muds and pore fluids on the seamount flanks.*

Transport conditions of muds and pore fluids are remarkably variable on the flanks and in the summit regions of the seamounts. Changes in the density and porosity of mudflows on the flanks of the seamounts indicates that compaction is not the only force that affects trends in these physical properties with depth. Additionally, deformation by gravitational sliding (Oakley et al., 2007) may affect these profiles, as well as continued serpentinization and alteration to other phases that significantly reduce porosity. Causes for these changes in physical properties will be assessed in shore-based mineralogical analysis and rheologic studies of whole-round samples. The latter were collected and preserved for mechanical, stress, and permeability testing, including the determination of physical properties.

6. *Provide a measure for comparing the nature of hydrologic characteristics (e.g., diffuse versus channelized fluid flow) on the flanks and summit regions of the mud volcanoes.*

Systematic variations in interstitial water composition profiles from flank sites indicate no significant vertical discharge of fluids. At each of the summit sites, pore fluid compositions show clear evidence of seepage at discharge rates in excess of the serpentinite matrix, which also is ascending and constructing the dome-like

features on the summit of two of the three cored seamounts. These results are consistent with published data that define the range and area of discharge at the summit sites.

7. *Determine the composition of fluid from depth and assess the type, extent, and effect of diagenetic reactions that occurred on the flanks of serpentinite mud volcanoes.*

Systematic variations in interstitial water composition profiles from Yinazao (13 km depth-to-slab), Fantangisña (14 km), and Asùt Tesoru (18 km) Seamounts augments previous results from South Chamorro (19 km) and Conical (18 km) Seamounts (Table **T1**). This combination of data reaffirms the dramatic change in the compositions of the slab-derived serpentinizing fluids as the slab descends (Mottl et al., 2004; Hulme et al., 2010). Dramatic differences include elevated Ca and Sr and low to extremely low K, Na, Cl, SO_4, B, and Na/Cl in fluids from Yinazao Seamount and, to a lesser extent, Fantangisña Seamount. In contrast, discharging fluids from Asùt Tesoru Seamount have a composition similar to that from South Chamorro and Conical Seamounts, with extremely high pH (up to 12.4), Ca and Sr depletions, and marked enrichments in carbonate alkalinity, DIC, DOC, NH_4, Na, K, Na/Cl, and B. Na concentrations are higher at Asùt Tesoru Seamount than at any the five seamounts mentioned above. Chemical compositions of pore water from the flank sites are consistent with a mixture of slab-derived fluid and seawater. Superimposed on this mixture are diagenetic changes that are evident in some of the measured chemical species.

Coupled to the seventh objective was the desire to document the composition of dissolved gases, specifically H_2, CH_4, and C_2H_6. Compositions of these gases differed from site to site, providing a measure of deep-sourced fluid composition. High concentrations of H_2, CH_4, and C_2H_6 were observed at the summit of Asùt Tesoru Seamount, and comparatively low but significant levels were detected at both summit and flank sites at Yinazao Seamount. Concentrations of H_2 and CH_4 show two distinct groupings of data: serpentinization-driven H_2 production and methane production. The relationship between methane and ethane data from Asùt Tesoru, South Chamorro, and Conical Seamounts converge on a single composition that may represent the hydrocarbon values produced by abiotic (Fisher Tropsch Type) synthesis in the deep-sourced fluid.

8. *Collect samples for the study of microbial/viral community interactions in materials bathed in deep-sourced fluids, distal serpentinite mud flows, and the underlying forearc pelagic sediment.*

Whole-round samples collected for microbiological studies were subsampled for shore-based analyses to explore the limits of microbial life in serpentinized mud using cultivation-based and cultivation-independent molecular biological approaches, microscopy, and assays for the detection of viruses. Postexpedition analyses will include an array of microbial community–level interrogation techniques: (1) total cell counts to quantify microbial biomass; (2) cultivation (including FACS high-throughput media screening and detection of adaptation to physical parameters such as pressure tolerance); (3) molecular analyses, including SSU ribosomal gene amplicon sequencing (to address community structure in greater detail), functional gene detection, and quantification through qPCR and single-cell genomics (to specifically address individual cell contributions); (4) metagenomics of the entire microbial community and metatranscriptomics of the most highly expressed genes to establish metabolic potential and deeper ecological and evolutionary relationships; and (5) viral counts and diversity. The only microbial analysis conducted at sea was to assess the quality of the whole rounds via tracer analysis. Tracers were pumped into the drill string prior to and during core recovery. Systematic sampling of the cored material and overlying surficial fluids indicates that most of the whole-round samples for microbiology are suitable for continued shore-based analyses.

9. *Complete initial fabrication of borehole structures for future in situ experiments and observations.*

Three casing strings, each with three or more joints of screened casing, were deployed, one in each of the summits of the cored serpentinite mud volcanoes. These casing strings form the foundation for a future deployment of CORK-lites (Wheat et al., 2012), which allow for a range of experiments and observations to be conducted simultaneously within a single structure that is open to deep-sourced fluids. We collected a water sample and measured temperature within two of the three newly deployed cased boreholes days after the bottom was sealed with cement. The recovered fluids were a mixture of seawater (drilling fluids) and deep-sourced fluid, and temperatures were higher than expected based on measurements collected during sediment coring operations. Combined, these data indicate that both boreholes tapped a hydrologic zone and active fluid discharge exists. The third site also should have active discharge based on systematic variations in interstitial water composition profiles that indicate fluid discharge rates of centimeters to tens of centimeters per year in the summit area. Similar results were observed at South Chamorro Seamount, which supports a CORK (Hole 1200C) with active fluid discharge. During Expedition 366, we visited Hole 1200C to remove the CORK body. Most of the CORK body from Hole 1200C was removed, leaving the sleeve joint that allows access to the CORK, but it retains the 3.25 inch diameter. Thus, with future funding and ROV operations, a network of four cased borehole systems will exist that span a range of distances from the trench, representing a range of pressure and temperature conditions at depth and different compositions of deep-sourced fluids. Such a transect will be instrumental to in situ experimentation and future monitoring to study, for example, processes associated with material (e.g., rocks, fluid, and mud) flow and alteration (e.g., abiotic and biotic reactions).

Operations

Table **T2** (expedition 366 hole summary) summarizes Expedition 366 operations.

Guam port call

Expedition 366 officially began with the first line ashore at Dock F-3 in Guam at 0648 h on 8 December 2016. Actions for the port call were to complete the change out of the top drive motor, which failed on the last site of the previous expedition, and replace the cryogenic magnetometer, which required *JOIDES Resolution* Science Operator (JRSO) technical staff with third-party support from 2G Enterprises. Loading included 1000 metric tons of marine gas oil (MGO), 20 metric tons of barite, and 20 metric tons of sepiolite drilling mud via local P-trucks, 58 joints (3 flats) of 10¾ inch 40.5 lb/ft buttress casing, 2 Baker-Hughes-Inteq drilling motors, 2 HOC DTU950 underreamers, and 3 standard reentry cones. Refrigerated containers carrying nearly 7 km of Expedition 363 cores were dispatched to the Kochi Core Repository in Japan, and returning surface freight was dispatched including the rental mud motor, an HOC DTU950 underreamer for refurbishment, and other miscella-

neous freight. Originally, the *JOIDES Resolution* was scheduled to depart at 0700 h on Tuesday, 13 December. However, due to military operations taking place in the area that morning, the decision was made with the pilot to depart at 0500 h.

Transit to Site 1200

The last line was cast off at 0518 h on 13 December 2016, and the transit proceeded without incident. The ship arrived at Site 1200 at 1624 h the same day.

Site 1200

Hole 1200C

After an 11 h transit from Guam, the vessel arrived at Site 1200 (proposed Site MAF-4B; 13°47.0724′N, 146°0.1717′E; water depth = 2932 m) at 1624 h on 13 December 2016. Planned operations at Hole 1200C were to remove the currently installed CORK and ROV platform, install a new ROV platform, and deploy the WSTP beyond the drill string to the depth of the screened portion of the cased hole to collect pristine formation fluid and measure a temperature profile for calculating the natural rate of fluid discharge from the borehole.

The recovery attempt began at 0500 h on 14 December, and several near misses occurred when the tool appeared to go over the top of the CORK head but the pipe heaved off before the J-slots were fully engaged. After 5.25 h, the CORK head was engaged and the recovery tool J-slots were fully engaged. However, the CORK head parted while attempting to pull it free of the reentry structure. Less than 10,000 lb of overpull was applied to get the CORK latch to shift; however, it failed at the latch assembly. Video of the reentry cone after removal showed a small diameter tube protruding from the center of the reentry cone. This was interpreted to be a piece of PVC tubing that had been previously installed in the CORK via ROV in 2009 after the original thermistor string was recovered in 2003. The high-resolution camera with the new upgraded pan, tilt, and zoom capability proved to be effective during the CORK recovery and assessment.

At 1615 h, the recovery tool with the recovered portion of the CORK returned to the rig floor. Science party microbiologists and geochemists sampled macrofauna and precipitates from the CORK head. Because the original CORK platform was not recovered and because the lower portion of the CORK remained in the hole, replacement of the ROV landing platform and the WSTP water sampling could not take place, and preparations were made to transit to Site U1491.

Site U1491

The ship transited 137 nmi to Site U1491 (proposed Site MAF-16A) in 14.5 h at an average speed of 9.8 kt, arriving in the area of Site U1491 at 1050 h on 15 December 2016.

Hole U1491A

A precision depth recorder (PDR) seafloor depth measurement was taken once the ship was over the site coordinates. A PDR seafloor depth measurement was 4442 meters below sea level (mbsl), different from the calculated depth of 4500 mbsl. This difference was attributed to the slope geometry of the seamount's flank; the PDR 3.5 kHz reflection first arrival came from upslope rather than from directly under the ship. To be certain about the seafloor depth, the seafloor was tagged with the core bit. At 0645 h on 16 December 2016, the bit took weight at 4494 mbsl, starting Hole U1491A (15°47.1175′N, 147°8.4909′E; water depth = 4494 m). During the tagging process, sediment entered the bit and bottom-hole assembly (BHA) and was then collected with the APC core barrel from inside the BHA without the core barrel being fired. The core barrel was recovered at 0800 h with 1.3 m of recovery, including three distinct mudlines, likely resulting from ship heave causing the BHA to hop and tag the seafloor three or more times.

Hole U1491B

At 1015 h, Hole U1491B (15°47.1176′N, 147°8.4908′E; water depth = 4493 m) was started at a seafloor depth of 4492 mbrf. Oriented APC coring continued using the advance by recovery method penetrating to 19.4 mbsf and recovering 19.0 m of core (98%). Coring was halted due to the continued presence of coarse gravel. All cores were incomplete strokes. Formation temperature measurements using the APCT-3 were attempted at 13.2 and 19.4 mbsf. The drill string was pulled out of the hole, clearing the seafloor at 2325 h.

Hole U1491C

Hole U1491C (15°47.1940′N, 147°8.4119′E; water depth = 4519 m) is located 200 m northwest (downslope) of Hole U1491B, and coring started at 0025 h at a seafloor depth of 4519 mbsl. The first two cores were oriented APC cores, and then because of incomplete stroke we switched to the HLAPC and advanced by recovery for Cores 366-U1491C-3F through 8F. At no time did the barrel fully stroke, and recovery varied from 1 to 4.7 m, prompting a switch to XCB coring. XCB Core 9X required 70 min of rotating time to cut the core, as well as substantial effort to clean out 5 m of coarse gravel fill on the bottom prior to cutting the core. Core 9X contained only 0.27 m recovery due to a jammed piece of core in the XCB cutting shoe. A second XCB core barrel was deployed, and the bit was advanced to 43.9 mbsf, when the driller noticed a loss of torque and pump pressure. Two unsuccessful attempts were made to recover the core barrel, but the overshot did not engage the pulling neck on the barrel. Upon recovery of the sinker bar string, the overshot was found to have all shear pins intact, but the core line was damaged on both runs. Recognizing that something was wrong with the drill assembly (and fearing a BHA failure), the drill string was recovered back to the ship. We found that the BHA had failed and that the following were lost in the hole: the bit, a nonmagnetic drill collar, an APC/XCB outer core barrel assembly, and an XCB core barrel assembly. At 0000 h on 18 December 2016, the ship started the 9 km transit to Site U1492 in DP mode.

Site U1492

Hole U1492A

The ship arrived at Site U1492 (proposed Site MAF-15A) at 0730 h on 18 December 2016 after a 9 km transit from Site U1491 in DP mode. Two replacement drill collars and a new APC/XCB outer core barrel assembly were made up to replace those lost in Hole U1491B. The rig mechanic worked on the blower motor in the top drive for 3 h before the remainder of the BHA was assembled. The pipe trip to the seafloor began at 1630 h on 18 December. The camera was deployed for a seafloor survey, and the target, a seep marked by a previous ROV survey, was found immediately, so no further survey was required. The ship was offset 200 m to the north, and coring in Hole U1492A (15°42.6775′N, 147°10.6003′E; water depth = 3657 m) started at 0725 h on 19 December, establishing a seafloor depth of 3657 mbsl. After Core 366-U1492A-2H, further coring was conducted using the HLAPC for better recovery in the stiff serpentinite muds. While recovering 9F from 38.3 mbsf, the core line

became snarled in the oil saver due to a kink above the rope socket, most likely caused by the high ship's heave. At this point, we ceased coring in the hole, not far short of the 50 mbsf target depth, with 38.3 m cored and 38.5 m recovered. After slipping and cutting the drilling line, the oil saver was cleared of the tangled core line and the core line was reheaded.

Hole U1492B

Hole U1492B (15°42.6216′N, 147°10.6011′E; water depth = 3669 m), started at 0045 h on 20 December 2016, is located 100 m south of Hole U1492A and is the second in the minitransect of holes at this site. The seafloor depth was 3669.1 mbsl, 12.5 m deeper than at Hole U1492A. Coring continued using the HLAPC coring system through Core 366-U1492B-13F to 51.4 mbsf with 52.0 m recovered, completing the objective at this hole.

Hole U1492C

At 1100 h on 21 December 2016, the ship was offset 120 m south to start Hole U1492C (15°42.5590′N, 147°10.6001′E; water depth = 3666 m) with a seafloor depth of 3666.5 mbsl. HLAPC coring continued through Core 366-U1492C-23F to 98.7 mbsf. Formation temperature measurements (APCT-3) were made during Cores 3F, 6F, 9F, 13F, 16F, 19F, and 22F (9.5, 23.5, 33.6, 51.7, 65.8, 73.9, and 94.0 mbsf, respectively). Coring was suspended at this point to allow deployment of the temperature dual-pressure tool (T2P) on the motion decoupled hydraulic delivery system (MDHDS). The hole was swept with 20 barrels of high-viscosity mud while the tools were being rigged up and prepared for deployment on the rig floor. The hole had been stable up to that point with no fill on connections or overpull coming off bottom. It took less than 1 h to rig up the MDHDS/T2P/Electrical Release System (ERS) tools, but while stabbing the logging line through the blocks (without rotation or circulation), the hole became unstable. The line was quickly pulled back out, and the driller fought to maintain rotation, with top drive torque increasing from 200 to over 500 A. It was agreed that the T2P deployment should be abandoned for this site and retried at a shallower depth at the next summit drill site (U1496). The hole was swept with 20 barrels of high-viscosity drilling mud, and a wiper trip was made to 70.6 mbsf to try and get some of the dense cuttings either out of the hole or below the bit so they could be ground to a finer grain size and circulated out of the hole. Coring resumed at 0200 h on 23 December. HLAPC Cores 24F through 28G were cut to 117.5 mbsf before high torque and overpull necessitated a second wiper trip. The next 13.75 h were spent on hole conditioning before it was considered safe enough to install the sinker bars and recover the XCB wash barrel, which contained ghost Core 28G (ghost cores come from an interval that has been previously penetrated). Coring then proceeded using the XCB coring system to recover Cores 29X through 30X to 129.4 mbsf. While cutting Core 31X at 139.1 mbsf, the driller once again lost rotation. The next 2.5 h were spent working to free the pipe; we then decided to abandon further attempts to core Hole U1492C, and the drill pipe was pulled up to the rig floor. We cored 139.1 m and recovered 72.0 m in Hole U1492C.

Hole U1492D

At 0935 h on 24 December 2016, preparations began for deploying the reentry cone/drill-in casing system for Hole U1492D (15°42.5694′N, 147°10.5991′E; water depth = 3666 m). The previously assembled standard reentry cone was moved over well center on the moonpool doors. The casing shoe joint and four 39 ft screened casing joints were assembled, followed by 13 additional 10.75 inch casing joints. The casing string was lowered and latched into the reentry cone. The stinger assembly was made up, including a tricone bit, a Baker-Hughes Inteq high-torque mud motor, a set of HOC underreamers, and the Dril-Quip (DQ) running tool. The motor/underreamer combo was tested in the moonpool for proper operation. At 0630 h on 25 December, the driller began lowering the reentry cone/casing assembly to the seafloor. Several QA/QC issues were identified during the making up of the casing and drilling assembly, including (1) an improperly machined thread on a casing joint, (2) a ~0.020 inch under gauge 16 inch casing hanger that prevented connection to the DQ running tool until 3 h of grinding work enabled them to fit together, (3) one of the other 16 inch casing hangers that was also found to be out of specification, and (4) the first set of HOC DTU950 underreamers that failed to open and close properly during the predeployment test at the usual 30–35 strokes/min, requiring instead 80 strokes/min to open and a pressure in excess of 700 psi. This underreamer was set aside and another was picked up; it performed normally.

Hole U1492D was started at 1620 h on 25 December at a tagged seafloor depth of 3666 mbsl, the same depth as for Hole U1492C. The drill-in casing method employed here used a mud motor to power rotation of the bit and underreamer bit assembly, which projects ~3 m below the bottom of the casing. The casing is 10.75 inch in diameter, the screened casing joints are 12.5 inch in diameter, and the underreamer arms were set to create a 14.75 inch diameter hole. Drilling proceeded smoothly until a harder layer was encountered at ~84 mbsf, a similar depth to a hard (but unrecovered) layer encountered while coring in Hole U1492C. The bit caught on this layer, causing the drill pipe to torque up and then detorque in the opposite direction when the bit was freed. On one such detorque, the pipe rotated enough to activate the casing running tool and release the reentry cone, and the reentry cone fell down the casing string and onto the seafloor over the hole. Shortly after this, at 0230 h on 26 December, the 211 m long casing string also disengaged from the casing running tool and dropped about 3 m. We could still drill ahead, and we were able to reengage the casing and penetrate to 93 mbsf. However, hole conditions remained poor, and it was decided to pull the casing back to the ship and inspect the casing and drilling assemblies. On recovery, one cone was missing from the underreamer, but other parts of the assemblies were in working order. The casing string was hung off in the moonpool forward of well center.

Given the difficulties drilling into serpentinite mud containing rock clasts in this hole, we decided on a different approach. We decided to first drill the hole without coring to 225 mbsf using a 14.75 inch bit and then reenter this hole and drill in the casing using the mud motor and underreamer bit. At 1415 h on 27 December, Hole U1492D was reentered and reamed down to the previous total depth of 93 mbsf. From that point, it took 17 h to advance the 14.75 inch bit to the target depth of 225 mbsf (11 m deeper than casing to provide an adequate amount of rathole). The drill bit was raised to 67 mbsf then run back down to 225 mbsf, and the hole was swept three times with high-viscosity mud to clean out cuttings prior to pulling this bit out of the hole to prepare for our second attempt to install casing.

At 0930 h on 29 December, the rig crew moved the already assembled casing string back to the center of the moonpool, reassembled the mud motor and underreamer, and then lowered the casing and drilling assembly to the seafloor. Hole U1492D was reentered for the second time at 2300 h. The casing was lowered to 54 mbsf before taking weight, and then drilling/washing with the underreamer continued slowly to 144 mbsf, where the casing became

stuck. Freeing the casing took 6 h. After further slow progress was halted at 184 mbsf by poor hole conditions, the bit was pulled back to 96 mbsf to free the casing. We resumed drilling it in and were able finally to drill all the way to the total target depth of 214 mbsf at an average rate of 10 m/h; the casing shoe is at 211 mbsf. The casing running tool was released at 2240 h. It was not possible to confirm that the latch ring on the casing hanger had fully engaged the reentry cone because clouds of cuttings and drilling mud obscured our camera images, but this lack of confirmation was not considered to be a significant problem for the installation. The drill string was raised back to the ship and was on the rig floor by 0915 h on 1 January 2017.

Three tasks remained to make the cased hole ready for a future deployment of borehole monitoring equipment: (1) clean the hole of any accumulated debris, (2) install a bridge plug at its base, (3) and install an ROV landing platform. A drilling BHA was lowered to the seafloor and reentered Hole U1492D to clean out any material that built up in the base of the casing. No obstructions were found to 211 mbsf, and a 30 barrel high-viscosity mud sweep made sure the hole was clear. The BHA was raised back to the ship, the bottom part was exchanged to include the bridge plug deployment apparatus, and Hole U1492D was reentered. The bridge plug was to be set near the base of the casing to prevent formation muds from coming up into the casing. However, at 2300 h on 2 January, while the pipe was hung off at the rotary for a pipe connection, the drill string jolted, suggesting that the drill string had become attached to the casing. After completing the pipe connection, it was confirmed that the mechanical bridge plug had set prematurely at a depth of 37 mbsf. After an unsuccessful attempt to unseat the bridge plug, the drill pipe was detached from it and raised back to the ship, where the bridge plug release tool was inspected. Nothing was found to be wrong with the running tool. The prevailing theory is that during the pipe trip through the water column, the running tool setting ring rotated the 10 required turns. Then, after reentry, when the pipe was hung off on the elevator stool, the ship took a large heave and the slips on the bridge plug hung up in the gap between casing joints (opposite the coupling), which allowed the appropriate amount of force to be applied, causing the slips on the bridge plug to set. Because removal of the bridge plug required preparation time, we decided to move on to Site U1493 at the foot of Asùt Tesoru Seamount, and return to Site U1492 later in the expedition. The drill string and positioning beacon were recovered, and the 136 nmi sea passage to Site U1493 began by 1430 h on 3 January.

We arrived back at Hole U1492D at 2130 h on 19 January, after a 50 nmi, 5 h transit from Site U1497. Hole U1492D was reentered at 0740 h on 20 January with the purpose of hammering out the bridge plug. The bridge plug was tagged at 40 mbsf, and it was hammered using a custom-built tool over a period of 3 h before it gave way and moved downhole. The pipe was lowered, and we relocated the bridge plug at 211 mbsf, just below the base of casing. The ROV landing platform was deployed by freefall, landing very close to centered in the reentry cone. The base of casing was cemented with 5 barrels of 14 lb/g cement. Cementing became the expedition's preferred method of sealing the base of casing because of the risk of the mechanical bridge plugs setting prematurely. The casing at Site U1492D is ready for future deployment of borehole monitoring instruments. The ship departed at 0200 h on 21 January for the 144 nmi transit to Hole U1496C.

Site U1493

Hole U1493A

The ship arrived at Site U1493 (proposed Site MAF-14A; 17°59.1668′N, 147°06.0057′E; water depth = 3359 m) at 0400 h on 4 January 2017 following a 136 nmi, 13 h transit from Site U1492. A reentry cone was set up in the moonpool in preparation for its use at Site U1496 at the summit of Asùt Tesoru Seamount, and the drill pipe was lowered through it. Sites U1493–U1496 form a ~14 km south-to-north transect from the foot to the summit and are close enough for transit between them in DP mode, which allowed the same drill string to be used without being raised back up to the ship. Owing to the time taken to deploy casing Hole U1492D, we scaled back the drilling plan for the Asùt Tesoru flank sites (U1493–U1495) to a single 50 m APC/ XCB hole at each of these three sites. While taking the first core, the APC core barrel bent in two places. This core recovered 9 cm of mud with microfossils, and we decide to offset a short distance to avoid the hard zone or rock that caused the bent core barrel at this location.

Hole U1493B

The ship was offset 10 m east, and we started Hole U1493B (17°59.1665′N, 147°06.0060′E; water depth = 3359 m) at 1800 h on 4 January 2017. Coring in Hole U1493B penetrated to 32.6 m. An APCT-3 measurement was made on Core 366-U1493B-5F at 24.5 mbsf, obtaining a satisfactory temperature equilibration curve. Because of slow coring due to difficult APC/XCB drilling conditions and because we had sufficient samples for lithologic, geochemical, and microbiological assessment of the site, we decided to stop after Core 9X and move 4 nmi upslope to Site U1494. Hole U1493B penetrated 32.6 m and recovered 19.0 m (58%). The transit started at 1615 h on 5 January in DP mode.

Site U1494

Hole U1494A

The ship arrived at Site U1494 at 2050 h on 5 January 2017 after at 4 nmi transit from Site U1493 in DP mode. The first core at Hole U1494A (18°03.00896′N, 147°06.0003′E; water depth = 2200 m) was taken at 2325 h, and HLAPC and XCB coring became progressively more difficult with depth. After Core 366-U1494-11X took 2 h to drill, we decided end the hole and move on to Site U1495. Hole U1494A penetrated 39.0 m and recovered 29.6 m (76%). The short transit to Site U1495 started at 2135 h on 6 January.

Site U1495

Hole U1495A

The ship arrived at Site U1495 at 0115 h on 7 January 2017. It quickly became apparent that the hole was unstable for drilling, and after each HLAPC core an XCB barrel was deployed and the bit drilled down to the depth of the previous HLAPC core. These XCB hole cleaning runs recovered two ghost cores containing mostly rock clasts. Elevated levels of hydrogen were found in Core 366-U1495A-2F, so we decided to core a second hole at this site to increase the number of microbiological and interstitial water samples across this interval. Hole U1495A (18°05.6693′N, 147°06.0004′E;

water depth = 1406 m) penetrated 10.7 m and recovered 5.3 m (76%).

Hole U1495B

The vessel was offset 25 m northwest, and Hole U1495B (18°05.6788′N, 147°05.9901′E; water depth = 1402 m) was started at 1320 h. The water depth here was 1403 mbsl, 3 m shallower than Hole U1495A. Coring continued with the HLAPC coring system to a total depth of 10.8 mbsf. Once again, hole cleaning and a slow rate of penetration drilling out the HLAPC rathole led us to stop coring this hole. Hole U1495B penetrated 10.8 m and recovered 10.8 m (100%). The transit to Site U1496 in DP mode began at 2100 h.

Site U1496

Hole U1496A

Coring at Hole U1496A (proposed Site MAF-11A; 18°6.5936′N, 147°6.0999′E; water depth = 1244 m) began at 0045 h on 8 January 2017 after a 1 nmi transit from Site U1495. We started with HLAPC coring and switched to XCB coring after Core 366-U1496A-9F did not achieve a full stroke. Penetration rate slowed, and after reaching 44.8 mbsf, we ended the hole. Hole U1496A penetrated to 44.8 mbsf and recovered 38.7 m (86%).

Hole U1496B

Hole U1496B (18°6.6210′N, 147°6.1000′E; water depth = 1240 m) was started 50 m north of Hole U1496A at 1915 h on 8 January 2017. Coring proceeded well until a clast-rich zone starting at about 28 mbsf slowed coring. To try to pass through the zone, we took XCB Core 366-U1496B-8X, then drilled ahead to 34.3 mbsf and took Core 10F, which contained only rock clasts, so we ended the hole at this point. Hole U1496A penetrated to 36.0 mbsf and recovered 22.9 m (64%). To reach the target depth of about 110 mbsf at this site, we pulled the drill pipe back up to the ship to switch to RCB coring in a new hole.

Hole U1496C

Hole U1496C (18°6.6074′N, 147°6.1000′E; water depth = 1244 m) started at 2320 h on 9 January 2017 at a location midway between the first two holes at the site. Coring progressed quickly, penetrated 105 m, and recovered 8.52 m (8%). The low levels of core recovery were anticipated for rotary coring in this material, and the coring did its intended job of reaching 105 mbsf, the depth to which casing would be emplaced in the hole. The hole was swept and reamed, the reentry cone was deployed, and the drill pipe was raised back to the ship. To further prepare the hole for casing, it was reentered at 2340 h on 10 January with a 14.75 inch bit and was widened by drilling and reaming to 120 mbsf. The drill pipe was raised up to the drill floor, and the 105 m long casing was assembled.

The casing for Hole U1496C consisted of two regular 10.75 inch casing joints, three screened casing joints, and three further regular casing joints connected to a 16 inch casing hanger at the top. The underreamer and mud motor BHA was assembled and lowered through the casing, and the running tool on the BHA was attached to the casing hanger on the casing. The bit extended about 4 m below the base of casing. The casing and bit/underreamer assembly reentered Hole U1496C at 0130 h on 12 January and reached the target depth of 109 mbsf at 1100 h. Progress was fairly rapid, apart from taking a few hours to pass through a hard zone at ~40 mbsf. The casing was latched to the reentry cone, and the bit/underreamer assembly was pulled inside the casing. The ~4 m diameter circular ROV platform was deployed and landed slightly off-center by about 30 cm, but it is still functional. Hard fill was found in the casing at 99 mbsf, indicating that formation material had come up about 6 m inside the casing. The drill pipe was raised up to the ship, and the rig floor was secured for transit to Site U1497.

We returned to Hole U1496C on 21 January at 1525 h after a 144 nmi, 13.4 h transit from Hole U1492D. The aim was to take a water sample using the WSTP, remove the fill, and cement the bottom of the casing. The drill pipe was lowered to the seafloor and reentered Hole U1496C without difficulty, despite having to pass through the 32 inch diameter central aperture in the ROV landing platform. The drill pipe was lowered to 42 mbsf, within the upper joint of screened casing, where the WSTP was deployed to sample borehole fluids and take temperature measurements. Initial geochemical measurements of the ~1 L WSTP fluid sample indicate that it is mostly formation water, mixed with some drilling water (seawater). We used a 9.825 inch polycrystalline diamond (PDC) coring bit because it was narrow enough to fit inside the casing. The drill pipe was lowered, and we found fill at 99 mbsf, ~7 m above the base of casing, a similar depth to where it was when the casing was installed on 12 January. We sampled the material inside the casing with Cores 366-U1496C-12G and 13G, which recovered 7.7 m serpentinite mud with lithic clasts from this previously cored depth interval. Five barrels of 14 lb/g cement were pumped with the aim of sealing the base of casing. The drill pipe was raised above the seafloor, flushed to remove any residual cement, and then raised back to the ship, concluding operations at Site U1496.

Site U1497

Hole U1497A

The 94 nmi transit to Site U1497 (proposed site MAF-9B) took 9 h at 10.4 kt. Site U1497 is located near the summit of Fantangisña Seamount and is known from previous ROV dives to have more surface boulders and cobbles than the other two seamounts drilled during this expedition. Prior to starting the hole, we surveyed the seafloor with the subsea camera to find preferred coring locations with fewer surface rocks. Hole U1497A (16°32.2538′N, 147°13.2641′E; water depth = 2020 m) began at 1915 h on 13 January 2017 and reached 34.2 mbsf using a combination of HLAPC and XCB coring. After each HLAPC core, we reamed/drilled down to the base of advancement of the previous HLAPC core, during which we recovered additional core material (ghost cores). Hole U1497A cored 34.2 m and recovered 23.4 m (70%).

Hole U1497B

Hole U1497B (16°32.2528′N, 147°13.2606′E; water depth = 2019 m) started at 1530 h on 14 January 2017; it reached 25.1 mbsf and recovered 23.8 m (95%). It was decided to stop the hole at this point because of difficult drilling, and the bit was raised clear of the seafloor at 0005 h on 15 January.

Hole U1497C

Hole U1497C (16°32.2504′N, 147°13.2500′E; water depth = 2019 m) started at 1145 h on 15 January 2017 with the aim to drill down with a 14.75 inch bit to about 120 mbsf and then deploy screened casing in this predrilled hole for future borehole monitoring at this site. However, we stopped this hole at 12 mbsf because of high torque and slow penetration.

Hole U1497D

For a second attempt to drill a 14.75 inch hole to 120 mbsf, we started Hole U1497D (16°32.2548′N, 147°13.2621′E; water depth = 2020 m) 5 m north of where Hole U1497B had achieved reasonable penetration. Hole U1497D reached 120 mbsf at a slow but steady average rate of 7 m/h. The formation was firm, and the hole appeared to be in good condition, apart from a difficult zone in the upper part of the hole, perhaps related to loose sand and gravel observed in Hole U1497A between 23–26 mbsf. The hole was swept with 50 barrels of high-viscosity mud to prepare for installing the screened casing. The reentry cone was deployed by freefall, and then the drill pipe was raised back up to the ship.

The rig crew assembled the 106 m long casing string, including three joints of 10.75 inch casing, three joints of screened casing, and three further joints of 10.75 inch casing. The regular casing joints underneath the screened section provided space for cement to seal the bottom of the casing to prevent the formation from entering. The mud motor and underreamer assembly was lowered through the casing string, and the running tool on the drill pipe was attached to the hanger at the top of the casing. The bit and underreamer extended ~4 m below the base of the casing. The whole assembly was lowered to the seafloor, and Hole U1497D was reentered at 2310 h on 17 January 2017. At 1230 h on 18 January, the casing had been successfully installed to 107 mbsf in Hole U1497D. During the installation, it took ~5 h to pass below a difficult zone at ~40 m. Then at ~70 mbsf, the casing prereleased from the running tool, falling ~15 m farther down the hole (a similar prerelease happened at Hole U1492D earlier in the expedition), but we were able to continue washing and reaming down to the target depth. The hole was swept with high-viscosity mud, and the drill pipe and underreamer assembly was raised back up to the ship.

The cementing BHA reentered Hole U1497D and was lowered to 105 mbsf, where 5 barrels of 14 lb/g cement was pumped down to seal the bottom of the casing at that depth. The drill pipe was raised above the seafloor, and the drill pipe was flushed to remove any residual cement. The bit was at the rig floor at 1540 h on 19 January, and the ship prepared for transit. The positioning beacon would not release from the seafloor, but we planned to return to Hole U1497D to check the location of the cement plug later in the expedition and to try to retrieve the beacon using a grapple hook.

We returned to Hole U1497D at 2045 h on 22 January after a 95 nmi, 9 h transit. Hole U1497D was reentered at 0325 h on 23 January, and the drill pipe was lowered to 24 mbsf, in the middle of the top joint of screened casing, where the WSTP was deployed to sample borehole fluids and take temperature measurements. The drill pipe was lowered further to check the location of the cement plug, now that it had time to harden. The top of cement was tagged at 103 mbsf, about 4 m above the base of the casing. The cement plug is therefore well positioned to stop the formation entering into the casing. The ROV landing platform was deployed by freefall. On our previous visit to Site U1497, the beacon failed to release, so we now fished it manually using a grappling hook that had been attached to the subsea camera frame for this purpose. This concluded operations at Site U1497.

Site U1498

Hole U1498A

The ship transited 6 nmi in DP mode to Site U1498 (proposed Site MAF-10B) in 9 h from the Fantangisña Seamount summit, arriving at 2300 h. We had moved the location of Hole U1498A (16°27.0898′N, 147°09.8502′E; water depth = 3497 m) ~1300 m southwest (downslope) from the planned location to the toe of the slope where the serpentinite mud flows are thinner and where drilling could reach the underlying sediments more easily/quickly in the remaining operation time. An RCB coring assembly was lowered and tagged the seafloor at 3497 mbsl at 0615 h on 24 January. The steep (~25%) slopes at the foot of the mud volcano cause underestimated seafloor depths when calculated from PDR or the seismic seafloor reflection, and the bathymetric data for the site location proved to be more accurate. Cores 366-U1498A-1R through 19R penetrated 182 m and recovered 21 m (11%). Coring was faster below 45 mbsf, in the nannofossil-bearing volcanic ashes that underlie the serpentinite mudflows. Following low recovery, we ended Hole U1498A at 182 mbsf and moved ~700 m northeast, upslope, to a location where the serpentinite mud flows are thicker.

Hole U1498B

At 0300 h on 26 January 2017, the seafloor at Hole U1498B (16°27.3716′N, 147°10.1166′E; water depth = 3285 m) was tagged with the drill pipe, and the tag was observed with the subsea camera to confirm the water depth and check seafloor conditions on the lower slope of Fantangisña Seamount. Seafloor depth from the bathymetry was within 1 m of the tagged seafloor depth at this hole. Cores 366-U1498B-1R through 27R penetrated 260 m and recovered 83 m (32%). In the upper five cores, the RCB coring system preferentially recovered hard rock clasts, and below this depth, recovery of serpentinite muds increased with depth. Drilling was slow until we drilled through to the underlying sediments in the middle of Core 23R at 205 mbsf. We stopped drilling when the hole reached 260 mbsf, and the last core of the expedition came on deck at 1730 h on 29 January. Enough operation time remained for downhole logging, so the drill bit was raised up to 52 mbsf, and we logged the hole with the triple combo tool string, comprising magnetic susceptibility, NGR, resistivity, and caliper tools. The tool string reached 229 mbsf, 31 m from the base of the hole. Magnetic susceptibility, NGR, resistivity, and temperature data were recorded for one downward pass and two upward passes of the tool string. The logging data cover the transition from the sediments to the overlying serpentinite mudflows and up to the base of the drill pipe. The tools were rigged down by 0530 h on 30 January, and the drill pipe was raised back to the ship by 1250 h. The rig was secured, and the transit to Hong Kong began at 1530 h on 30 January.

Transit to Hong Kong port call

The 1917 nmi transit to Hong Kong took 7.8 days at an average speed of 10.3 knots. We proceeded to Hong Kong East Lamma Channel pilot station for a timed arrival for the scheduled pilot boarding time of 0700 h on 7 February 2017.

Education and outreach

Two education and outreach personnel participated on Expedition 366. Many of their interactions with students were in the form of live video broadcasts, YouTube videos, blogs, and Facebook posts. About 40 live video broadcasts with classrooms were conducted, reaching an estimated 1500 students and teachers. Survey responses from participants indicated that they found the objectives of the expedition clearly explained; they learned about science content, process, and careers; presentations were presented at the appropriate level for the audience; and programs exceeded their

expectations. Respondents also indicated that the programs helped them to meet their relevant state and local education standards. Based on additional written comments and thank-you notes from teachers, these broadcasts had a positive impact on the students. Several teachers mentioned that they used the YouTube video series prior to these broadcasts to introduce students to the scientific goals of the expedition.

Two series of short YouTube videos were produced. One series showcased research conducted by individual scientists or teams of scientists (Science Spotlights). The other series was a personal take on life on board the *JOIDES Resolution*, highlighting holiday activities, different parts of the ship, and other updates (Video Diaries). All videos were aimed at increasing ocean science understanding and awareness, particularly among middle school and college students, and secondarily among the broader audience that follows *JOIDES Resolution* via the website or social media. Twelve videos were completed, with a total of 1945 views prior to departing the ship. These videos will continue to be available indefinitely as a resource through USSSP's YouTube channel.

The education and outreach team also published 45 blogs to the *JOIDES Resolution* website, with a total of 5806 reads prior to departing from the ship (ranging from 160 to 1025 reads per blog). These blogs cover everything from science activities to the ship, shipboard life, weather, and a range of topics of interest to the general public. The public provided many comments to these blogs.

In addition to these media connections, the education and outreach team created two focused projects. One included the creation of a 3-D model of a serpentinite mud volcano made to scale, including an accurate representation of the layers beneath the volcano. It was used for live broadcasts and will be used in a German school by one of the education and outreach team members.

The second project was centered on a small 360 camera. The camera was placed in various spaces around the ship to record research activity. Some of the 360 videos and photos were posted to Facebook and received positive feedback and engagement. Although it was difficult to incorporate 360 video into other video projects and live broadcasts, due to technological constraints, the concept has broad appeal. We hope IODP will continue to integrate this technology into future outreach efforts. The TAMU-based computer specialists will look into possible technical applications for future outreach activities.

Education and outreach activities will continue ashore. Both team members plan on submitting articles for publication and expanding current blogs to connect deep-sea scientific drilling to other aspects of marine science. Lastly, both team members will participate in a workshop. The German team member will participate in IODP Expedition at Geo-Show in Braunschweig on 15 March 2017, held simultaneously with the 2017 ICDP/IODP Symposium in Germany. The US Outreach Officer will participate in USSSP's booth and teacher outreach activities at the National Science Teachers Association annual conference in Los Angeles on 29 March–2 April 2017.

References

.Athy, L.F., 1930. Density, porosity, and compaction of sedimentary rocks. *AAPG Bulletin,* 14(1):1–24. **http://archives.datapages.com/data/bulletns/1917-30/images/pg/00140001/0000/00010.pdf**

Bekins, B.A., and Dreiss, S.J., 1992. A simplified analysis of parameters controlling dewatering in accretionary prisms. *Earth and Planetary Science Letters,* 10(3–4)9:275–287. **http://dx.doi.org/10.1016/0012-821X(92)90092-A**

Bhanot, K.K., Downes, H., Petrone, C.M., and Humphreys-Williams, E., in press. Textures in spinel peridotite mantle xenoliths using micro-CT scanning: examples from Canary Islands and France. *Lithos.* **http://dx.doi.org/10.1016/j.lithos.2016.08.004**

Curtis, A.C., Wheat, C.G., Fryer, P., and Moyer, C.L., 2013. Mariana forearc serpentinite mud volcanoes harbor novel communities of extremophilic Archaea. *Geomicrobiology Journal,* 30(5):430–441. **http://dx.doi.org/10.1080/01490451.2012.705226**

Desprairies, A., 1982. Authigenic minerals in volcanogenic sediments cored during Deep Sea Drilling Project Leg 60. *In* Hussong, D.M., Uyeda, S., et al., *Initial Reports of the Deep Sea Drilling Project,* 60: Washington, DC (U.S. Government Printing Office), 455–466. **http://dx.doi.org/10.2973/dsdp.proc.60.120.1982**

Fryer, P., 2012. Serpentinite mud volcanism: observations, processes, and implications. *Annual Review of Marine Science,* 4(1):345–373. **http://dx.doi.org/10.1146/annurev-marine-120710-100922**

Fryer, P., Gharib, J., Ross, K., Savov, I., and Mottl, M.J., 2006. Variability in serpentinite mudflow mechanisms and sources: ODP drilling results on Mariana forearc seamounts. *Geochemistry, Geophysics, Geosystems,* 7(8):Q08014. **https://doi.org/10.1029/2005GC001201**

Fryer, P., Pearce, J.A., Stokking, L.B., et al., 1990. *Proceedings of the Ocean Drilling Program, Initial Reports,* 125: College Station, TX (Ocean Drilling Program). **http://dx.doi.org/10.2973/odp.proc.ir.125.1990**

Fryer, P., Wheat, C.G., and Mottl, M.J., 1999. Mariana blueschist mud volcanism: implications for conditions within the subduction zone. *Geology,* 27(2):103–106. **http://dx.doi.org/10.1130/0091-7613(1999)027<0103:MBMVIF>2.3.CO;2**

Fryer, P.B., and Salisbury, M.H., 2006. Leg 195 synthesis: Site 1200—serpentinite seamounts of the Izu-Bonin/Mariana convergent plate margin (ODP Leg 125 and 195 drilling results). *In* Shinohara, M., Salisbury, M.H., and Richter, C. (Eds.), *Proeedings of the Ocean Drilling Program, Scientific Results,* 195: College Station, TX (Ocean Drilling Program), 1–30. **http://dx.doi.org/10.2973/odp.proc.sr.195.112.2006**

Gharib, J., 2006. Clastic metabasites and authigenic minerals within serpentinite protrusions from the Mariana forearc: implications for subforearc subduction processes [Ph.D. dissertation]. University of Hawaii.

Haggerty, J.A., 1991. Evidence from fluid seeps atop serpentine seamounts in the Mariana forearc: clues for emplacement of the seamounts and their relationship to forearc tectonics. *Marine Geology,* 102(1–4):293–309. **http://dx.doi.org/10.1016/0025-3227(91)90013-T**

Haggerty, J.A., and Chaudhuri, S., 1992. Strontium isotopic composition of the interstitial waters from Leg 125: Mariana and Bonin forearcs. *In* Fryer, P., Pearce, J.A., Stokking, L.B., et al., *Proceedings of the Ocean Drilling Program, Scientific Results,* 125: College Station, TX (Ocean Drilling Program), 397–400. **http://dx.doi.org/10.2973/odp.proc.sr.125.124.1992**

Haggerty, J.A., and Fisher, J.B., 1992. Short-chain organic acids in interstitial waters from Mariana and Bonin forearc serpentines: Leg 125. *In* Fryer, P., Pearce, J.A., Stokking, L.B., et al., *Proceedings of the Ocean Drilling Program, Scientific Results,* 125: College Station, TX (Ocean Drilling Program), 387–395. **http://dx.doi.org/10.2973/odp.proc.sr.125.125.1992**

Hulme, S.M., Wheat, C.G., Fryer, P., and Mottl, M.J., 2010. Pore water chemistry of the Mariana serpentinite mud volcanoes: a window to the seismogenic zone. *Geochemistry, Geophysics, Geosystems,* 11(1):Q01X09. **http://dx.doi.org/10.1029/2009GC002674**

Johnson, L.E., and Fryer, P., 1990. The first evidence for MORB-like lavas from the outer Mariana forearc: geochemistry, petrography and tectonic implications. *Earth and Planetary Science Letters,* 100(1–3):304–316. **http://dx.doi.org/10.1016/0012-821X(90)90193-2**

Krastel, S., Spiess, V., Ivanov, M., Weinrebe, W., Bohrmann, G., Shashkin, P., and Heidersdorf, F., 2003. Acoustic investigations of mud volcanoes in the Sorokin Trough, Black Sea. *Geo-Marine Letters,* 23(3–4):230–238. **http://dx.doi.org/10.1007/s00367-003-0143-0**

Lenoir, X., Garrido, C.J., Bodinier, J.-L., and Dautria, J.-M., 2000. Contrasting lithospheric mantle domains beneath the Massif Central (France) revealed by geochemistry of peridotite xenoliths. *Earth and Planetary Science Letters,* 181(3):359–375. **http://dx.doi.org/10.1016/S0012-821X(00)00216-8**

Lever, M.A., Torti, A., Eickenbusch, P., Michaud, A.B., Šantl-Temkiv, T., and Jørgensen, B.B., 2015. A modular method for the extraction of DNA and RNA, and the separation of DNA pools from diverse environmental sample types. *Frontiers in Microbiology,* 6:1–25. **http://dx.doi.org/10.3389/fmicb.2015.00476**

Lockwood, J.P., 1972. Possible mechanisms for the emplacement of alpine-type serpentinite. *Memoir - Geological Society of America,* 132:273–288. **http://dx.doi.org/10.1130/MEM132-p273**

Maekawa, H., Shozui, M., Ishii, T., Fryer, P., and Pearce, J.A., 1993. Blueschist metamorphism in an active subduction zone. *Nature,* 364(6437):520–523. **https://doi.org/10.1038/364520a0**

McCollom, T.M., and Bach, W., 2009. Thermodynamic constraints on hydrogen generation during serpentinization of ultramafic rocks. *Geochimica et Cosmochimica Acta,* 73(3):856–875. **http://dx.doi.org/10.1016/j.gca.2008.10.032**

Mercier, J.-C.C., and Nicolas, A., 1975. Textures and fabrics of upper mantle peridotites as illustrated by xenoliths from basalts. *Journal of Petrology,* 16:454–487. **http://dx.doi.org/10.1093/petrology/16.2.454**

Mottl, M.J., 1992. Pore waters from serpentinite seamounts in the Mariana and Izu-Bonin forearcs, Leg 125: evidence for volatiles from the subducting slab. *In* Fryer, P., Pearce, J.A., Stokking, L.B., et al., *Proceedings of the Ocean Drilling Program, Scientific Results,* 125: College Station, TX (Ocean Drilling Program), 373–385. **http://dx.doi.org/10.2973/odp.proc.sr.125.121.1992**

Mottl, M.J., and Alt, J.C., 1992. Data report: minor and trace element and sulfur isotopic composition of pore waters from Sites 778 through 786. *In* Fryer, P., Pearce, J.A., Stokking, L.B., et al., *Proceedings of the Ocean Drilling Program, Scientific Results,* 125: College Station, TX (Ocean Drilling Program), 683–688. **http://dx.doi.org/10.2973/odp.proc.sr.125.184.1992**

Mottl, M.J., Komor, S.C., Fryer, P., and Moyer, C.L., 2003. Deep-slab fluids fuel extremophilic Archaea on a Mariana forearc serpentinite mud volcano: Ocean Drilling Program Leg 195. *Geochemistry, Geophysics, Geosystems,* 4:9009. **http://dx.doi.org/10.1029/2003GC000588**

Mottl, M.J., Wheat, C.G., Fryer, P., Gharib, J., and Martin, J.B., 2004. Chemistry of springs across the Mariana forearc shows progressive devolatilization of the subducting plate. *Geochimica et Cosmochimica Acta,* 68(23):4915–4933. **http://dx.doi.org/10.1016/j.gca.2004.05.037**

Oakley, A., 2008. A multi-channel seismic and bathymeric investigation of the central Mariana convergent margin [Ph.D. dissertation]. University of Hawaii. **http://www.soest.hawaii.edu/GG/resources/theses/Oakley Dissertation 2008.pdf**

Oakley, A.J., Taylor, B., Fryer, P., Moore, G.F., Goodliffe, A.M., and Morgan, J.K., 2007. Emplacement, growth, and gravitational deformation of serpentinite seamounts on the Mariana forearc. *Geophysical Journal International,* 170(2):615–634. **http://dx.doi.org/10.1111/j.1365-246X.2007.03451.x**

Oakley, A.J., Taylor, B., and Moore, G.F., 2008. Pacific plate subduction beneath the central Mariana and Izu-Bonin fore arcs: new insights from an old margin. *Geochemistry, Geophysics, Geosystems,* 9(6):Q06003. **https://doi.org/10.1029/2007GC001820**

Pons, M.-L., Quitté, G., Fujii, T., Rosing, M.T., Reynard, B., Moynier, F., Douchet, C., and Albarède, F., 2011. Early Archean serpentine mud volcanoes at Isua, Greenland, as a niche for early life. *Proceedings of the National Academy of Sciences of the United States of America,* 108(43):17639–17643. **http://dx.doi.org/10.1073/pnas.1108061108**

Reagan, M.K., Ishizuka, O., Stern, R.J., Kelley, K.A., Ohara, Y., Blichert-Toft, J., Bloomer, S.H., Cash, J., Fryer, P., Hanan, B.B., Hickey-Vargas, R., Ishii, T., Kimura, J.-I., Peate, D.W., Rowe, M.C., and Woods, M., 2010. Fore-arc basalts and subduction initiation in the Izu-Bonin-Mariana system. *Geochemistry, Geophysics, Geosystems,* 11(3):Q03X12. **http://dx.doi.org/10.1029/2009GC002871**

Savov, I.P., Guggino, S., Ryan, J.G., Fryer, P., and Mottl, M.J., 2005a. Geochemistry of serpentinite muds and metamorphic rocks from the Mariana forearc, ODP Sites 1200 and 778–779, South Chamorro and Conical Seamounts. *In* Shinohara, M., Salisbury, M.H., and Richter, C. (Eds.), *Proceedings of the Ocean Drilling Program, Scientific Results,* 195: College Station, TX (Ocean Drilling Program), 1–49. **http://dx.doi.org/10.2973/odp.proc.sr.195.103.2005**

Savov, I.P., Ryan, J.G., D'Antonio, M., and Fryer, P., 2007. Shallow slab fluid release across and along the Mariana arc-basin system: insights from geochemistry of serpentinized peridotites from the Mariana fore arc. *Journal of Geophysical Research: Solid Earth,* 112(B9):B09205. **http://dx.doi.org/10.1029/2006JB004749**

Savov, I.P., Ryan, J.G., D'Antonio, M., Kelley, K., and Mattie, P., 2005b. Geochemistry of serpentinized peridotites from the Mariana forearc Conical Seamount, ODP Leg 125: implications for the elemental recycling at subduction zones. *Geochemistry, Geophysics, Geosystems,* 6(1):Q04J15. **http://dx.doi.org/10.1029/2004GC000777**

Shervais, J.W., 1982. Ti-V plots and the petrogenesis of modern and ophiolitic lavas. *Earth and Planetary Science Letters,* 59(1):101–118. **http://dx.doi.org/10.1016/0012-821X(82)90120-0**

Shipboard Scientific Party, 1990. Site 780. *In* Fryer, P., Pearce, J.A., Stokking, L.B., et al., *Proceedings of the Ocean Drilling Program, Initial Reports,* 125: College Station, TX (Ocean Drilling Program), 147–178. **http://dx.doi.org/:10.2973/odp.proc.ir.125.108.1990**

Shipboard Scientific Party, 2002. Site 1200. *In* Salisbury, M.H., Shinohara, M., Richter, C., et al., *Proceedings of the Ocean Drilling Program, Initial Reports,* 195: College Station, TX (Ocean Drilling Program), 1–173. **http://dx.doi.org/10.2973/odp.proc.ir.195.103.2002**

Smith, D., 1977. The origin and interpretation of spinel-pyroxene clusters in peridotite. *Journal of Geology,* 85(4):476–482. **http://dx.doi.org/10.1086/628321**

Takai, K., Moyer, C.L., Miyazaki, M., Nogi, Y., Hirayama, H., Nealson, K.H., and Horikoshi, K., 2005. *Marinobacter alkaliphilus* sp. nov., a novel alkaliphilic bacterium isolated from subseafloor alkaline serpentine mud from Ocean Drilling Program Site 1200 at South Chamorro Seamount, Mariana forearc. *Extremophiles,* 9(1):17–27. **http://dx.doi.org/10.1007/s00792-004-0416-1**

Uyeda, S., and Horai, K., 1982. Heat flow measurements on Deep Sea Drilling Project Leg 60. *In* Hussong, D.M., Uyeda, S., et al., *Initial Reports of the Deep Sea Drilling Project,* 60: Washington, DC (U.S. Government Printing Office), 789–800. **http://dx.doi.org/10.2973/dsdp.proc.60.146.1982**

Uyeda, S., and Kanamori, H., 1979. Back-arc opening and the mode of subduction. *Journal of Geophysical Research: Solid Earth,* 84(B3):1049–1061. **https://doi.org/10.1029/JB084iB03p01049**

Wheat, C.G., Edwards, K.J., Pettigrew, T., Jannasch, H.W., Becker, K., Davis, E.E., Villinger, H., and Bach, W., 2012. CORK-lite: bringing legacy boreholes back to life. *Scientific Drilling,* 14:39–43. **http://dx.doi.org/10.2204/iodp.sd.14.05.2012**

Wheat, C.G., Fryer, P., Fisher, A.T., Hulme, S., Jannasch, H., Mottl, M.J., and Becker, K., 2008. Borehole observations of fluid flow from South Chamorro Seamount, an active serpentinite mud volcano in the Mariana forearc. *Earth and Planetary Science Letters,* 267(3–4):401–409. **http://dx.doi.org/10.1016/j.epsl.2007.11.057**

Wheat, C.G., Fryer, P., Takai, K., and Hulme, S., 2010. Spotlight 9: South Chamorro Seamount, 13°7.00′N, 146°00.00′E. *Oceanography*, 23(1):174–175. **http://www.tos.org/oceanography/issues/issue_archive/issue_pdfs/23_1/23-1_wheat.pdf**

Table T1. Critical parameters of the deep-sourced fluid from five Mariana serpentinite mud volcanoes. Depth to slab was determined by seismic reflection profile for Yinazao, Fantangisña, and Asùt Tesoro Seamounts (Oakley et al., 2007, 2008; Oakley, 2008), and by equilibrium mineral assemblages in metamafic clasts for South Chamorro and Conical Seamounts (Maekawa et al., 1993; Fryer et al., 2006; Gharib, 2006). Distance to trench and temperature of slab from Hulme et al. (2010). Depth to slab measurements for Yinazao, Fantangisna, and Asut Tesoro from Oakley et al. (2008) and Oakley (2008). Depth to slab measurements for South Chamorro and Conical are extrapolation estimates (see text). Pore water measurements from Expedition 366, Mottl et al. (2003, 1992), Mottl (2004), and Hulme et al. (2010).

Measurement	Yinazao	Fantangisña	Asùt Tesoro	South Chamorro	Conical
Distance to trench (km)	55	62	72	78	86
Depth to slab (km)	13	14	18	18	19
Temperature of slab (°C)	~80	~150	~250	250–350	250–350
Pore water pH	11.2	11.0	12.5	12.5	12.5
Pore water Ca (mM)	64	90	0.1	0.3	1
Pore water K (mM)	~1	5	14	19	15

Table T2. Expedition 366 hole summary.

Hole	Latitude	Longitude	Water depth (mbsl)	Cores (*N*)	Interval cored (m)	Core recovered (m)	Recovery (%)	Drilled interval (m)	Total penetration (m)	Time on hole (days)	Comments
1200C	13°47.0724′N	146°0.1717′E	2932.16	0			0.00			1.2	CORK recovery operation
U1491A	15°47.1175′N	147°08.4909′E	4493.68	1	1.3	1.32	101.54		1.3	0.81	
U1491B	15°47.1176′N	147°08.4908′E	4492.48	5	19.4	18.98	97.84		19.4	0.68	
U1491C	15°47.1940′N	147°08.4119′E	4518.88	9	34.2	23.08	67.49		34.2	1.34	
U1492A	15°42.6775′N	147°10.6003′E	3656.58	9	38.3	38.49	100.50		38.3	1.72	
U1492B	15°42.6216′N	147°10.6011′E	3669.10	13	51.4	52.03	101.23		51.4	1.43	
U1492C	15°42.5590′N	147°10.6001′E	3666.47	30	139.1	71.35	51.29		139.1	3.36	
U1492D	15°42.5694′N	147°10.5991′E	3666.44	0			0.00			9.79	
										1.19	Reoccupation of Hole U1492D
U1493A	17°59.1668′N	147°06.0057′E	3358.92	1	0.1	0.09	90.00		0.1	0.5	
U1493B	17°59.1665′N	147°06.0060′E	3358.92	9	32.6	19.03	58.37		32.6	1.44	
U1494A	18°3.0896′N	147°6.0003′E	2199.80	10	39.0	27.99	71.77		39.0	1.03	
U1495A	18°05.6693′N	147°06.0004′E	1405.81	3	10.7	4.84	45.23		10.7	0.62	
U1495B	18°05.6788′N	147°05.9901′E	1401.89	4	10.8	10.18	94.26		10.8	3.35	
U1496A	18°6.5936′N	147°6.0999′E	1243.38	10	42.8	38.36	89.63	2	44.8	0.66	
U1496B	18°6.6205′N	147°6.0998′E	1240.18	9	30.0	22.08	73.60	6	36.0	0.94	
U1496C	18°06.6068′N	147°06.1001′E	1243.17	11	105.0	8.52	8.11		105.0	3.78	
										0.85	Reoccupation of Hole U1496C
U1497A	16°32.2536′N	147°13.2642′E	2019.24	9	34.2	22.47	65.70		34.2	0.2	
U1497B	16°32.2528′N	147°13.2606′E	2018.22	6	23.8	19.91	83.66		23.8	0.56	
U1497C	16°32.2504′N	147°13.2500′E	2018.30	0			0.00			0.42	
U1497D	16°32.2548′N	147°13.2621′E	2018.80	0			0.00			8	
				0						0.71	Reoccupation of Hole U1497D
U1498A	16°27.0898′N	147°09.8502′E	3496.21	19	181.6	20.59	11.34		181.6	1.85	
U1498B	16°27.3716′N	147°10.1166′E	3284.70	27	260.0	82.82	31.85		260.0	4.83	
			Totals:	185	1054.3	482.13		8	1062.3		

Table T3. pXRF results for rock surfaces in Expedition 366 cores. **Download table in .csv format.**

Table T4. ICP-AES and pXRF shipboard data for serpentinized ultramafic clasts, serpentinite muds, and entrained metamorphosed mafic rocks chosen for full chemical analysis during Expedition 366. **Download table in .csv format.**

Table T5. Microbiological whole-round samples collected and preserved during Expedition 366.

Seamount	Hole	Samples obtained
Yinazao	U1491B	5
	U1491C	5
	Total:	10
	U1492A	9
	U1492B	12
	U1492C	16
	Total:	37
Asùt Tesoru	U1493B	5
	U1494A	7
	U1495A	2
	U1495B	2
	Total:	16
	U1496A	11
	U1496B	8
	U1496C	3
	Total:	22
Fantangisña	U1497A	4
	U1497B	6
	Total:	10
	U1498A	4
	U1498B	11
	Total:	15

Table T6. Heat flow estimates, Expedition 366.

Hole	Seamount	Gradient (°C/km)	Thermal conductivity (W/[m·K])	Heat flow (mW/m^2)
Summits				
U1492C	Yinazao	12.0	1.41	16.9
U1496A	Asùt Tesoru	14.2	1.25	17.8
U1497A	Fantangisña	11.7	1.43	16.8
1200A and 1200E	S. Chamorro	10.9	1.38	15.3
Flanks				
U1491B	Yinazao	20.6	1.48	30.5
U1493B	Asùt Tesoru	21.2	1.51	31.9
Sedimentary basin (DSDP Leg 60)				
459	Asùt Tesoru	28.6	1.09	30
458	Asùt Tesoru	25.9	1.12	25
Sites with flow				
1200F	S. Chamorro	72.4	1.38	101
U1492C	Yinazao	39.8	1.41	56
780	Conical	37.8	1.38	52

Figure F1. Location map of Expedition 366 Sites U1491–U1498 and Site 1200 on South Chamorro Seamount.

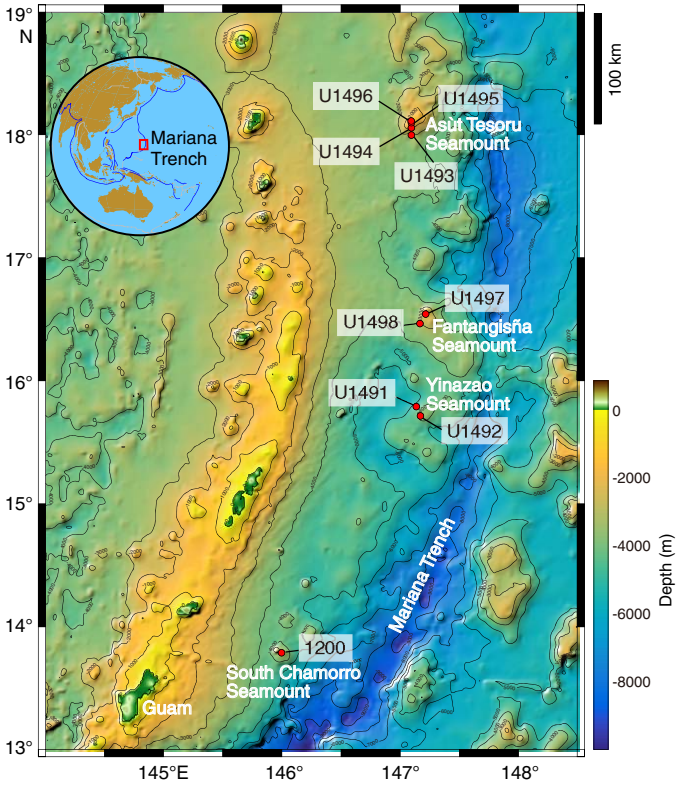

Figure F2. Idealized cross-section of the Mariana forearc setting, including the relative positioning of serpentinite mud volcanoes. Tectonic Zones 1–6 in the forearc subduction zone complex are keyed to core images in this figure and to photomicrographs in Figure **F3**. Figure modified after Fryer et al. (1999).

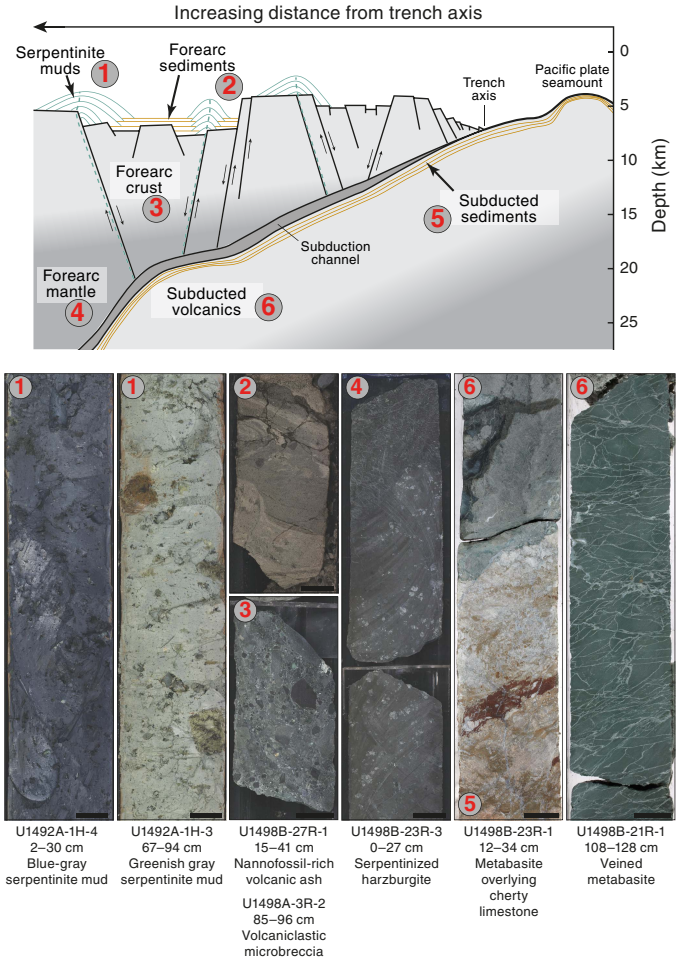

Figure F3. Representative samples keyed to zones and cores in Figure **F2**, Expedition 366. A. Discoasters (*D. variabilis*), coccoliths, and volcanic glass in volcanic ash deposits underlying Fantangisña Seamount (Zone 2). Microfossils establish an approximate age of 2.5 Ma for the sediments under the mud volcano, thus establishing the maximum age of onlap of the mudflows from this part of the volcano. B. Elliptical pale green glass bleb with prismatic orthopyroxene crystals in a microbreccia of presumed boninitic affinity (Zone 3; plane-polarized light [PPL]). opx = orthopyroxene. C. Mildly serpentinized porphyroclastic clinopyroxene (cpx)-bearing harzburgite (40% serpentinization) (Zone 4; cross-polarized light [XPL]). Strained, granulated olivine porphyroclasts retain optical continuity. Opx deformed with undulatory extinction. Cpx, commonly along opx margins, may be granule exsolution. Spinel (sp) penetrates other mineral grain boundaries. D. Blue serpentine forming pseudomorphic mesh textures (Zones 1–4; PPL). E. Ultracataclasite (Zone 5; PPL). Clasts of smeared chert (Ch) and fossiliferous siliceous limestone (Ls) within ultrafine-grained matrix. F. Euhedral-subhedral pink augite (Cpx) and plagioclase (Pl) showing equigranular texture (Zone 6; PPL). Labeled, altered plagioclase shows relict albite twin.

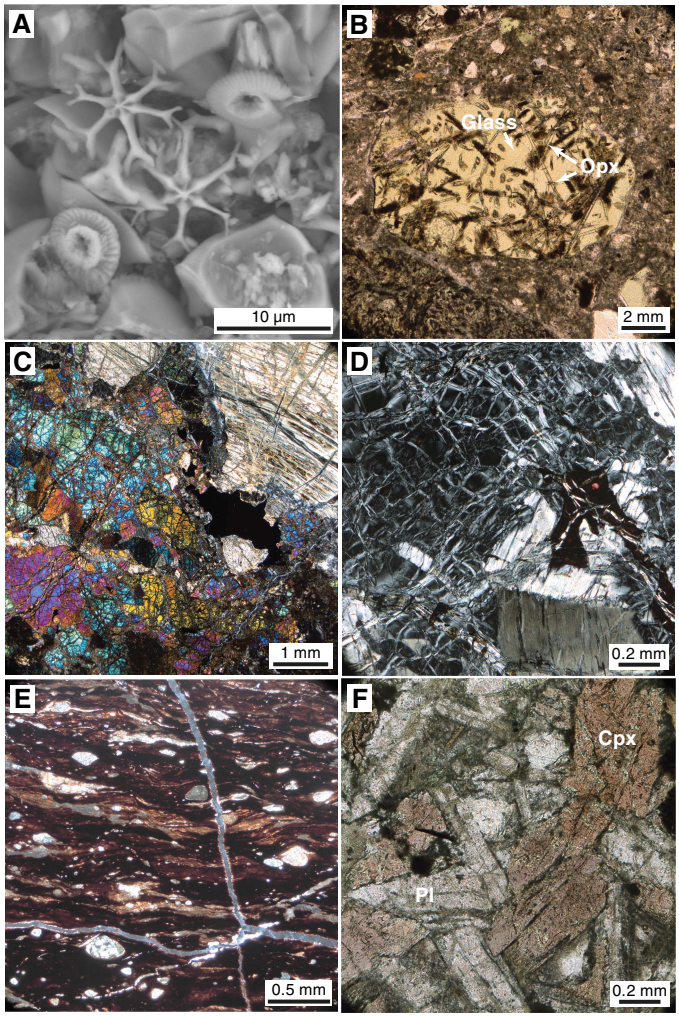

Figure F4. Major element variation of serpentinite muds and clasts, Expedition 366. Mafics = entrained metamorphosed mafic clasts. Green fields reflect range of values from serpentinized ultramafic rocks collected on Conical and South Chamorro Seamounts and analyzed by Savov et al. (2007).

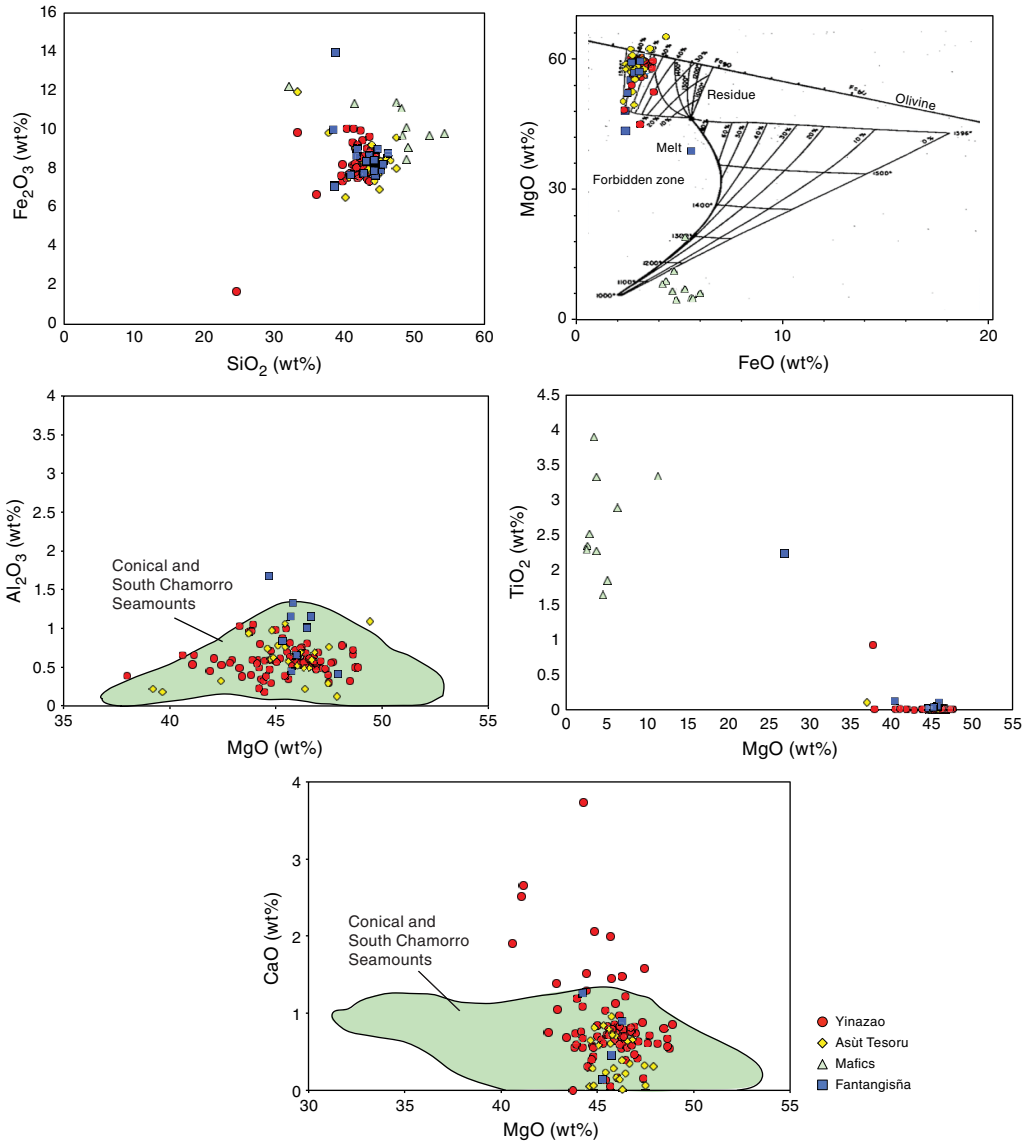

Figure F5. Immobile trace element variations in serpentinite muds and clasts, Expedition 366.

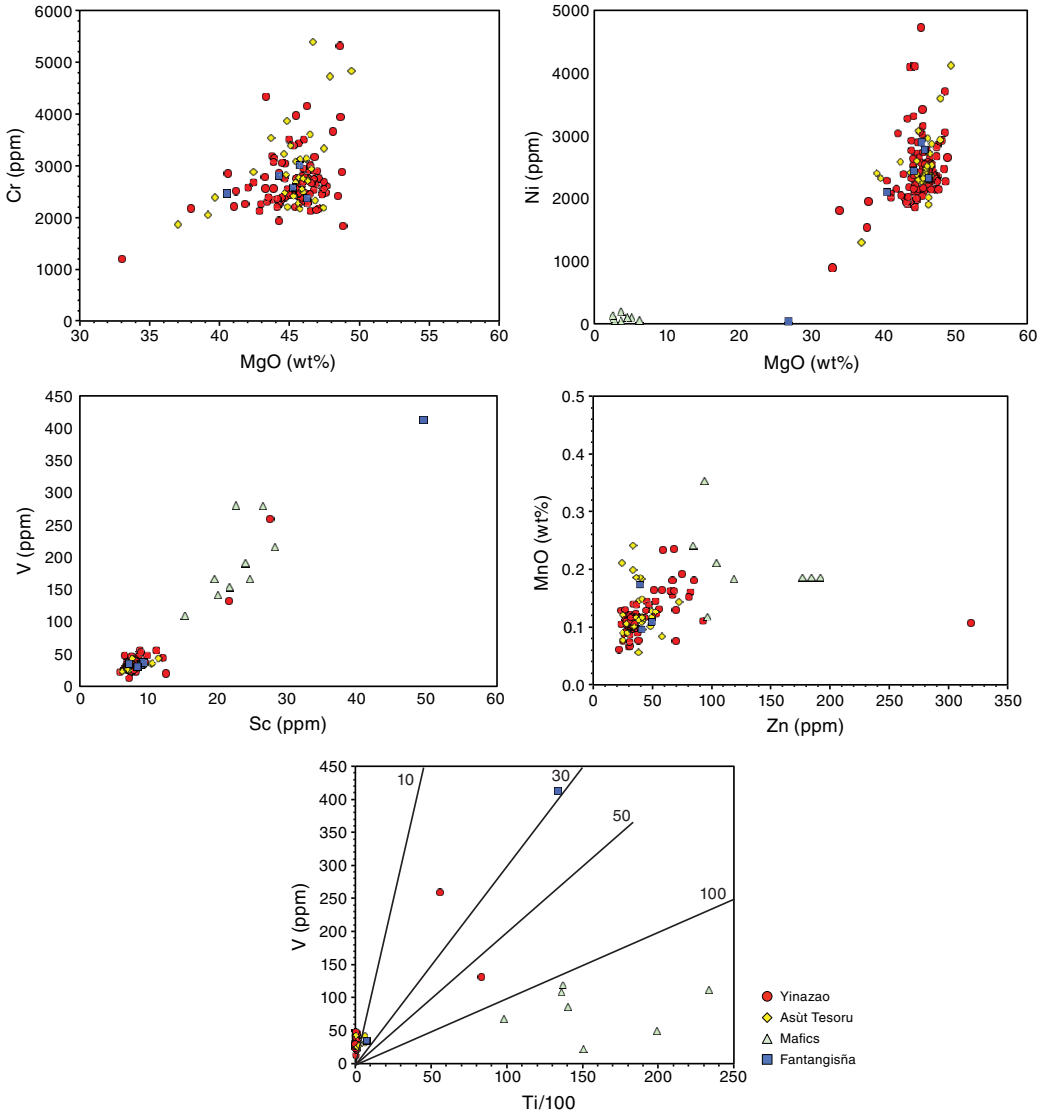

Figure F6. Variations of fluid-sensitive elements in serpentinite muds and clasts, Expedition 366.

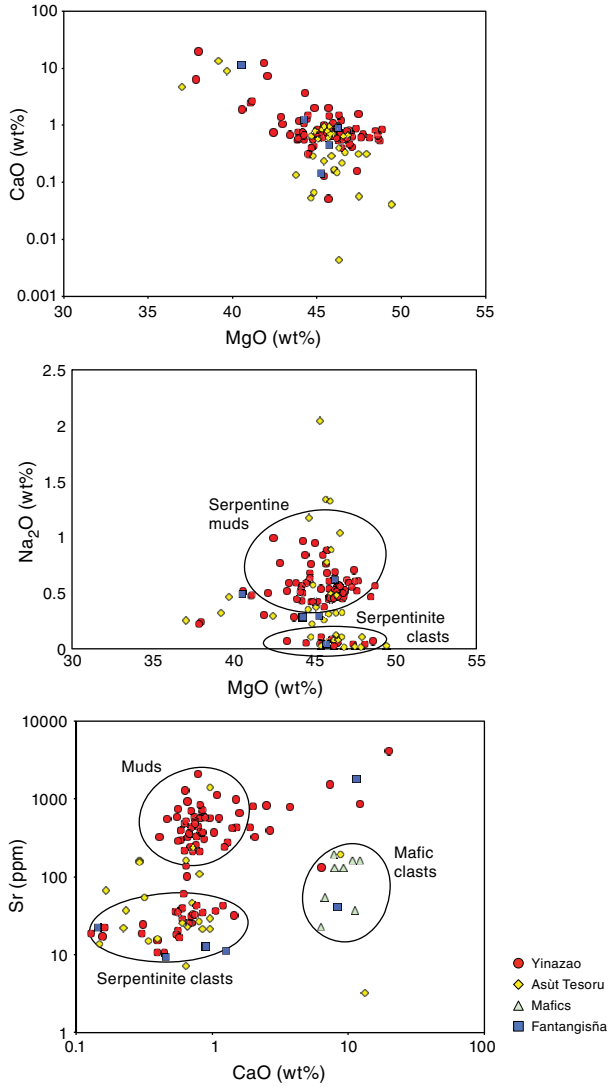

Figure F7. Elemental variations in metamorphosed mafic rocks compared to serpentinites, Expedition 366.

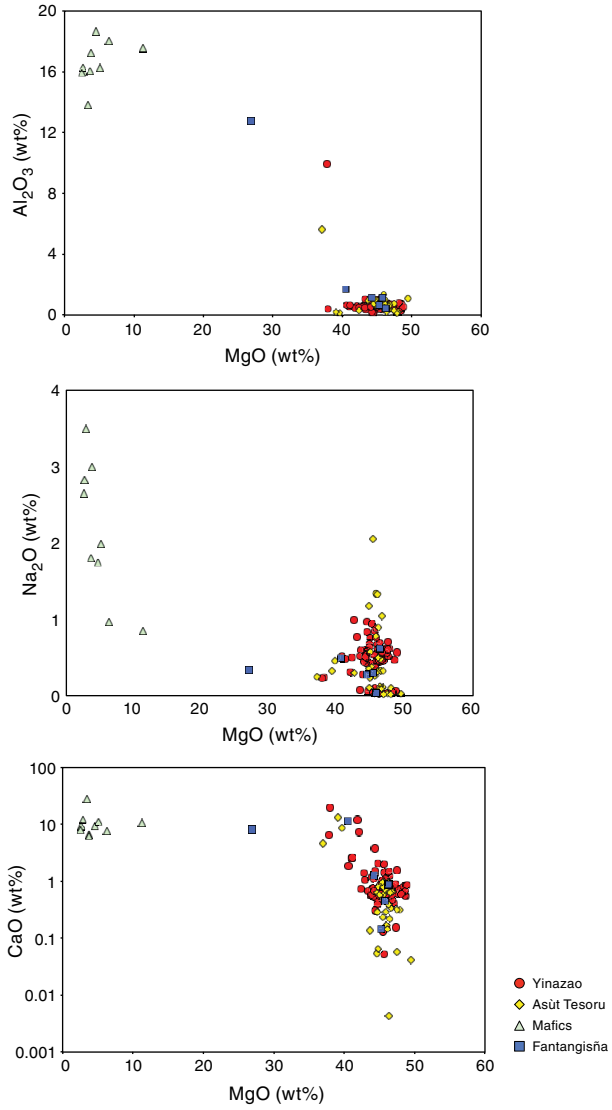

Figure F8. Gas compositions, Expedition 366. A. H_2 vs. CH_4, Yinazao and Asùt Tesoru Seamounts, Expedition 366. B. CH_4 vs. C_2H_6 diagram for Asùt Tesoru, Conical and South Chamorro Seamounts. Data for Conical and South Chamorro Seamounts from Shipboard Scientific Party (1990, 2002; respectively). Star = potential end-member composition.

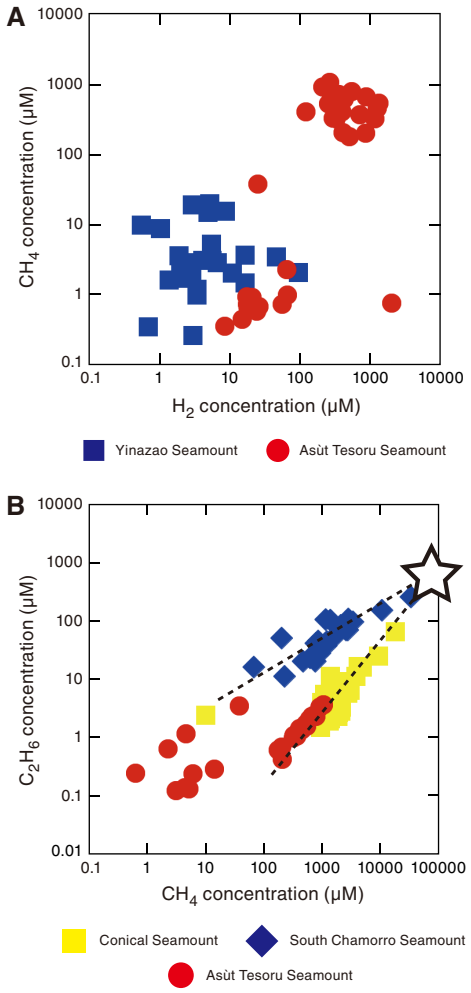

Figure F9. Selected pore water data, Expedition 366. Data for Conical and South Chamorro Seamounts are plotted for comparison to the summit sites (Hulme et al., 2010).

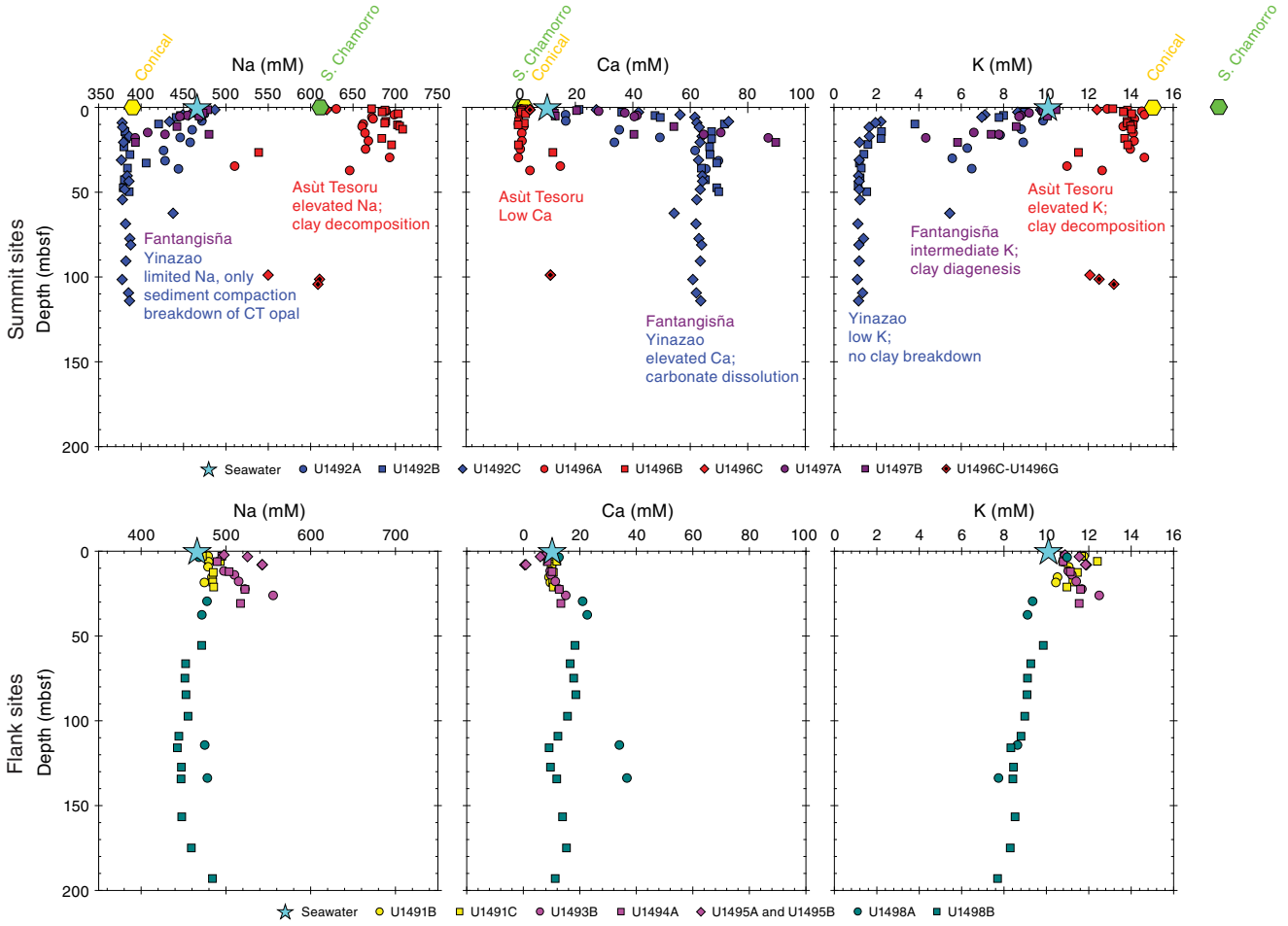

Figure F10. Map of Mariana forearc. Labeled seamounts are active serpentinite mud volcanoes. Shaded and colored regions show where expected reactions are thought to occur within the subduction channel.

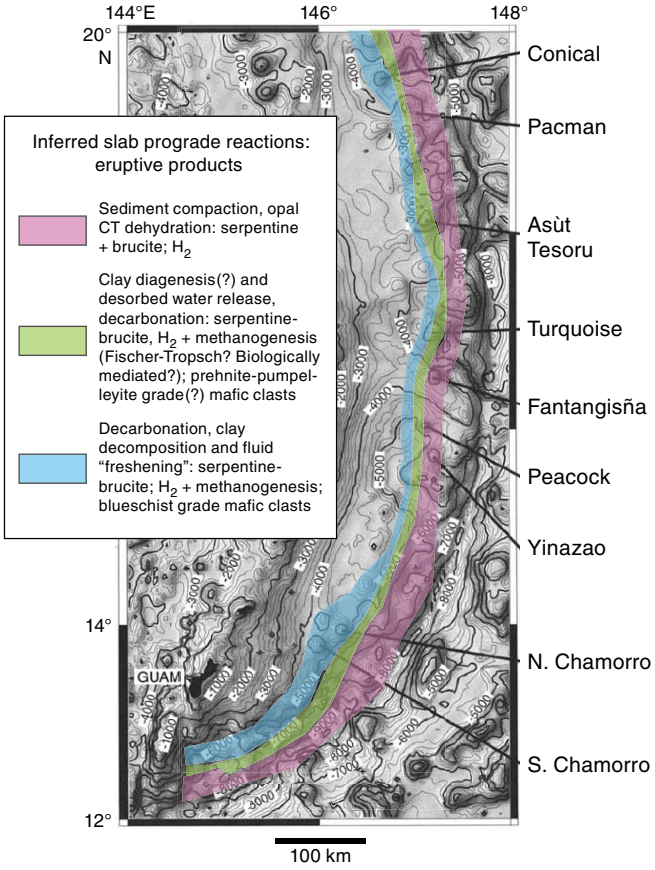

Figure F11. Idealized cartoon of the Mariana forearc with results from pore water chemical data derived during Expedition 366 and data from two other serpentinite mud volcanoes at a greater distance from the trench (South Chamorro and Conical Seamount). Slab devolatilization was identified through the compositions of pore fluids. Pore water data for Conical and South Chamorro Seamounts from Hulme et al. (2010). For ease of comparison, all elemental concentrations are plotted in millimolar, but B was multiplied by 10 and Na was divided by 10. Figure modified from Fryer et al. (1999).

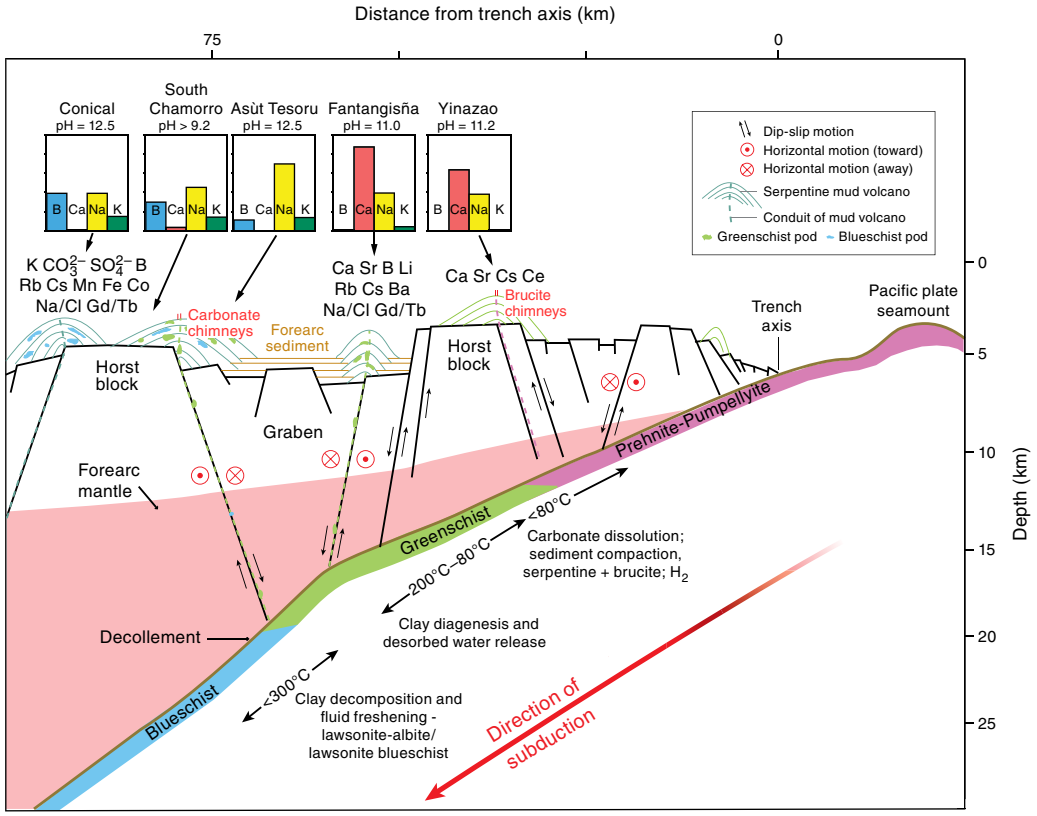

Figure F12. Porosity data from Expedition 366 sites with data from Leg 125. Expedition 366 summit sites are plotted in blue, and flank sites are plotted in red. Also shown are porosities from ODP Leg 125 Sites 778 and 779 (flank sites) and 780 (summit site). Green and yellow correspond to sites that differ from common flank or summit values, respectively.

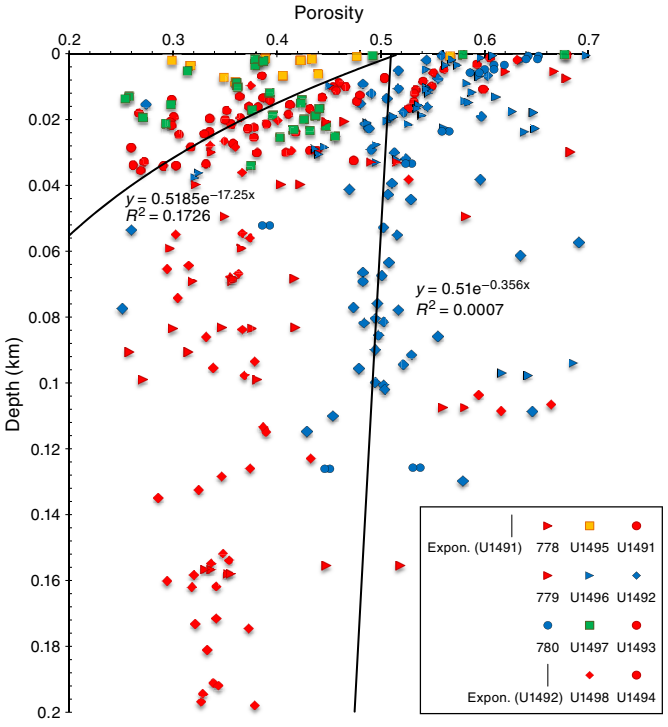

Figure F13. GRA density. A. Holes U1492A–U1492C. Data obtained below 100 mbsf are not plotted. B. Holes U1496A and U1496B.

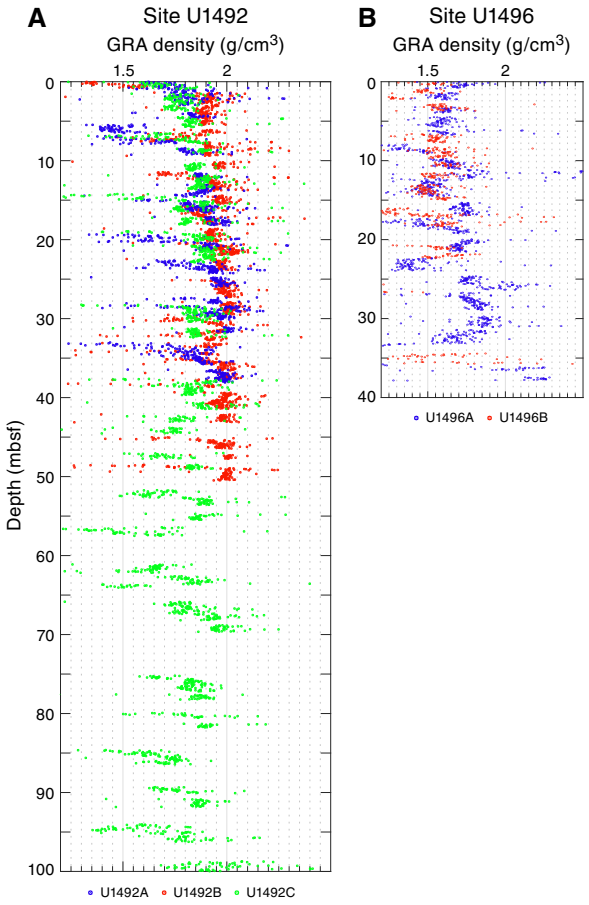

Figure F14. Calculated heat flow, Expedition 366. Values are derived from downhole APCT-3 formation temperatures and core-based thermal conductivity measurements. Published heat flow data from the area and similar geologic settings are shown for comparison.

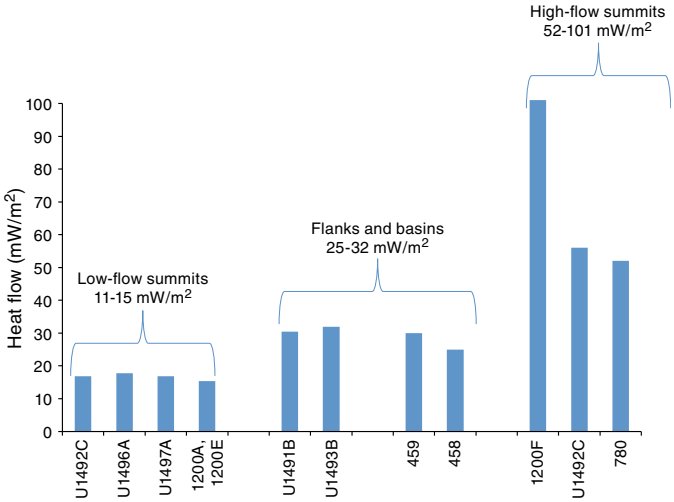

Figure F15. Magnetic susceptibility and magnetic intensity of the uppermost 40 m after 20 mT AF demagnetization, Expedition 366. All sites are included except Site U1495, which penetrated to only ~10 mbsf. High magnetic intensity relative to magnetic susceptibility in some cores and holes is likely due to drill string overprint. Asùt Tesoru holes have a higher average susceptibility than the other mud volcanoes